PX_4^+, $P_2X_5^+$, and $P_5X_2^+$ (X = Br, I) Salts of the Superweak $Al(OR)_4^-$ Anion [R = $C(CF_3)_3$]**

Marcin Gonsior,[a] Ingo Krossing,*[a] Lutz Müller,[a] Ines Raabe,[a] Martin Jansen,[b] and Leo van Wüllen[b]

Abstract: $PX_4^+[Al(OR)_4]^-$ (X = I: **1a**, X = Br: **1b**) was prepared from X_2, PX_3, and $Ag[Al(OR)_4]$ [R = $C(CF_3)_3$] in CH_2Cl_2 at −30 °C in 69–86 % yield. $P_2X_5^+$ salts were prepared from $2\,PX_3$ and $Ag[Al(OR)_4]$ in CH_2Cl_2 at −30 °C yielding almost quantitatively $P_2X_5^+[Al(OR)_4]^-$ (X = I: **3a**, X = Br: **3b**). The phosphorus-rich $P_5X_2^+$ salts arose from the reaction of cold (−78 °C) mixtures of PX_3, P_4, and $Ag[Al(OR)_4]$ giving $P_5X_2^+[Al(OR)_4]^-$ (X = I: **4a**, X = Br: **4b**) with a C_{2v}-symmetric P_5 cage. Silver salt metathesis presumably generated unstable PX_2^+ cations from PX_3 and $Ag[Al(OR)_4]$ (X = Br, I) that acted as electrophilic carbene analogues and inserted into the X–X (P–X/P–P) bond of X_2 (PX_3/P_4) leading to the highly electrophilic and CH_2Cl_2-soluble PX_4^+ ($P_2X_5^+$/$P_5X_2^+$) salts. Reactions that aimed to synthesize $P_2I_3^+$ from P_2I_4 and $Ag[Al(OR)_4]$ instead led to anion decomposition and the formation of $P_2I_5(CS_2)^+[(RO)_3Al\text{-}F\text{-}Al(OR)_3]^-$ (**5**). All salts were characterized by variable-temperature solution NMR studies (**3b** also by ^{31}P MAS NMR), Raman and/or IR spectroscopy as well as X-ray crystallography (with the exception of **4a**). The thermochemical volumes of the P–X cations are 121 (PBr_4^+), 161 (PI_4^+), 194 ($P_2Br_5^+$), 271 ($P_2I_5^+$), and 180 Å^3 ($P_5Br_2^+$). The observed reactions were fully accounted for by thermochemical calculations based on (RI-)MP2/TZVPP ab initio results and COSMO solvation enthalpy calculations (CH_2Cl_2 solution). The enthalpies of formation of the gaseous P–X cations were derived as +764 (PI_4^+), +617 (PBr_4^+), +749 ($P_2I_5^+$), +579 ($P_2Br_5^+$), +762 ($P_5I_2^+$), and +705 kJ mol^{-1} ($P_5Br_2^+$). The insertion of the intermediately prepared carbene analogue PX_2^+ cations into the respective bonds were calculated, at the (RI-)MP2/TZVPP level, to be exergonic at 298 K in CH_2Cl_2 by $\Delta_r G(CH_2Cl_2) =$ −133.5 (PI_4^+), −183.9 (PBr_4^+), −106.5 ($P_2I_5^+$), −81.5 ($P_2Br_5^+$), −113.2 ($P_5I_2^+$), and −114.5 kJ mol^{-1} ($P_5Br_2^+$).

Keywords: ab initio calculations · cations · halogens · phosphorus · subvalent compounds

Introduction

The knowledge on cationic or neutral binary P–X species in which X may be F, Cl, Br, I is still very sparse and limited to P^VX_5 (**A**, X = F, Cl), $P^VX_4^+$ (**B**, X = F–I),[1] $P^{III}X_3$ (**C**, X = F–I), $P^{III}{}_2I_5^+$[2, 3] (**D**), $P^{II}{}_2X_4$ (**E**, X = F, Cl, I), P_3F_5 (**F**), and very recently subvalent $P_3I_6^+$ ($P^{2.33}$)[4] (**G**; see Scheme 1). Solution studies showed the additional existence of small amounts of the phosphorus-rich cage molecules P_4Br_2 (**H**) and P_7I_3 (**I**) in CS_2 solutions of P_4 and X_2 mixtures (X = Br, I).[5]

Structural data are only available for types **A**–**E** and **G**. In the case of the cations **B**, **D**, and **G**, types **D** and **G** are only known for X = I. These binary phosphorus–iodine cations are very electrophilic, and $P_2I_5^+$ immediately decomposed the EF_6^- counterions when prepared from P_2I_4 and $I_3^+EF_6^-$ (E = As, Sb) at −78 °C furnishing only the decomposition products PF_3, EI_3, and I_2.[3] The same is true to a lesser extent for the more stable $PI_4^+EF_6^-$ salts.[1b, 6] The P–F bond energy (490 kJ mol^{-1} in PF_3)[7] is amongst the highest-known single-bond energies in the periodic table and therefore accounted for the decomposition reactions. To circumvent the decomposition of these fluorometalate anions, we employed a new generation of weakly basic anions of type $Al(OR)_4^-$ (R = perfluorinated organo ligand $C(CF_3)_3$)[8, 9, 22] that also appeared to be ideal spectator ions, since they allowed the unusual D_{2h}-symmetric $Ag(\eta^2\text{-}P_4)_2^+$ cation to be isolat-

[a] Priv. Doz. Dr. I. Krossing, M.Sc. M. Gonsior, Cand. Chem. L. Müller, Cand. Chem. I. Raabe
University of Karlsruhe, Engesserstr. Geb. 30.45
76128 Karlsruhe (Germany)
Fax: (+49) 721-608-48-54
E-mail: krossing@chemie.uni-karlsruhe.de

[b] Prof. Dr. M. Jansen, Dr. L. van Wüllen
Solid-state NMR spectroscopy:
Max-Planck Institut für Festkörperchemie
Heisenbergstr. 1, 70569 Stuttgart (Germany)

[**] Part of this work was presented at the Gordon Research Conference on Inorganic Chemistry in Newport, R.I. (USA), July 2001 and at the 25th Fluorine Conference of Japan, Fukuoka (Japan) November 2001.

Supporting information for this article is available on the WWW under http://www.chemeurj.org/ or from the author.

  0947-6539/02/0819-4475 $ 20.00+.50/0

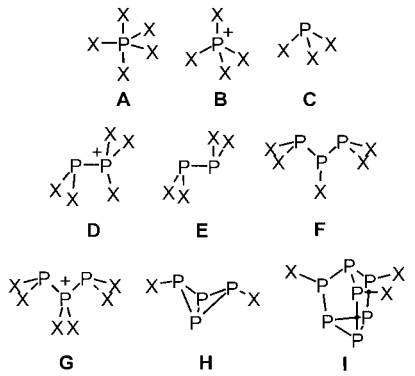

Scheme 1. Known neutral or cationic binary P–X species. Note that some species may only exist with one type of halide X.

ed.[10, 11, 12] Recently, we briefly showed[4] that P_2I_4 and PI_3 reacted with $Ag[Al(OR)_4]$[9, 13] to give $P_3I_6^+[Al(OR)_4]^-$.[4] A carbenoid "PI_2^+" cation was possibly an intermediate in this reaction. Here we investigated the insertion chemistry of the highly electrophilic carbene-analogous PX_2^+ cation (= PX_3 minus X^-; X = Br, I) into X_2, PX_3, and P_4 in more detail. Clean reactions leading to $PX_4^+[Al(OR)_4]^-$ (X = I: **1a**, X = Br: **1b**), $P_2X_5^+[Al(OR)_4]^-$ (X = I: **3a**, X = Br: **3b**), and $P_5X_2^+[Al(OR)_4]^-$ (X = I: **4a**, X = Br: **4b**) are presented. All species were fully characterized by experimental and theoretical methods. A preliminary account of $P_5X_2^+$ is given.[14]

Results and Discussion

Syntheses: The more basic[9] $Al[OC(H)(CF_3)_2]_4^-$ anion was tested in CH_2Cl_2 for some of the reactions given below. However, all reactions of $Ag[Al(OC(H)(CF_3)_2)_4]$ with PI_3 only led to full decomposition of the anion, even at low temperatures (−78 °C throughout), that is, the ^{31}P NMR spectra showed singlets that were tentatively assigned to $PI_x(OR)_{3-x}$ ($x = 0-3$) at $\delta(^{31}P) = 233.1$ ($x = 0$), 219.0 ($x = 1$), 140.2 ($x = 2$), and 173.9 ($x = 3$). Only with the less basic $Al[OC(CF_3)_3]_4^-$ anion[9, 11] did the reactions lead to the desired P–I cations and, therefore, in the following, R only denotes the perfluorinated $C(CF_3)_3$ ligand.

$PX_4^+[Al(OR)_4]^-$ **1a**,**b** (X = I: **1a**; X = Br: **1b**) was prepared in 69–86% yield by treating $Ag[Al(OR)_4]$,[13] PX_3, and X_2 according to Equation (1) in CH_2Cl_2 at −30 °C:

$$Ag[Al(OR)_4] + PX_3 + X_2 \rightarrow PX_4^+[Al(OR)_4]^-, \mathbf{1a,b} + AgX \quad (1)$$
$$R = C(CF_3)_3 \qquad X = I: \mathbf{1a}; X = Br: \mathbf{1b}$$

1a,**b** is less soluble than **3a**,**b** and **4a**,**b** below, and most of the dissolved **1a** (**1b**) from approximately 0.1 M solutions in CH_2Cl_2 precipitates upon storage at −30 °C (0 °C) overnight. Solutions of **1a**,**b** in CH_2Cl_2 and 1,2-$Cl_2C_2H_4$ are stable for at least three months at −30 °C, and those of **1a** may be handled briefly at RT. Solutions of **1b** start to slowly decompose at about 0 °C.[15] Solid **1a**,**b** is stable at RT for at least several days and much longer if stored at −30 °C.

Attempts were made to synthesize a $P_2I_7^+$ cation (i.e., I_3P-I^+-PI_3) according to Equation (2):

$$Ag[Al(OR)_4] + 2PI_3 + I_2 \rightarrow P_2I_7^+[Al(OR)_4]^-, \mathbf{2} + AgI \quad (2)$$
$$R = C(CF_3)_3$$

However, only $PI_4^+[Al(OR)_4]^-$ (**1a**) precipitated (unit cell determination and NMR) from the brown-red filtrate of this reaction, while solid PI_3 remained with the insoluble compounds (Raman). In an in situ ^{31}P NMR experiment, only the (broad) resonance of the PI_4^+ cation was visible at −90 °C (PI_3 is insoluble at this temperature).

$P_2X_5^+[Al(OR)_4]^-$ (**3a**,**b**) was conveniently prepared in 86 (X = I, **3a**) or 67% (X = Br: **3b**) yield by treating two equivalents of PX_3 with $Ag[Al(OR)_4]$[13] ([Eq. (3)] in CH_2Cl_2 ($T \leq -30$ °C):

$$Ag[Al(OR)_4] + 2PX_3 \rightarrow P_2X_5^+[Al(OR)_4]^-, \mathbf{3a,b} + AgX \quad (3)$$
$$R = C(CF_3)_3 \qquad X = I: \mathbf{3a}, X = Br: \mathbf{3b}$$

Although cold solutions of **3a**,**b** in 1,2-$Cl_2C_2H_4$ are stable, they may not be used as reaction media. 1,2-$Cl_2C_2H_4$ is a stronger and better chelating donor to the Ag^+ ion than CH_2Cl_2 and, therefore, the Ag^+ ion is less reactive and not capable of abstracting halide from PX_3 in 1,2-$Cl_2C_2H_4$ even at RT (cf. the very stable $[Ag(1,2\text{-}Cl_2C_2H_4)_3]^+[Al(OR)_4]^-$ structure in [9]). An in situ ^{31}P NMR spectrum of a PI_3 reaction in CD_2Cl_2 according to Equation (3) recorded immediately after all visible amounts of PI_3 were consumed only showed signals attributable to $P_2I_5^+$. However, $P_2I_5^+$ [→ P^{III}] slowly disproportionated in CH_2Cl_2 over several weeks, giving the reduced $P_3I_6^+$ [→ $P^{2.33}$] and another more highly oxidized species invisible on the timescale of NMR spectroscopy (see Equation (4) and below).

$$P_2I_5^+ \rightarrow P_3I_6^+ + ? \quad (4)$$

To obtain pure solid **3a**, one therefore has to filter the cold reaction solution immediately after all visible amounts of PI_3 have been consumed (approx. 1–2 h) and remove all volatile compounds to leave clean **3a** in quantitative yield (IR, elemental analysis).

$P_5X_2^+[Al(OR)_4]^-$ (**4a**,**b**) was prepared by reacting P_4, PX_3 and $Ag[Al(OR)_4]$[13] according to Equation (5) at −78 °C.

$$Ag[Al(OR)_4] + PX_3 + P_4 \rightarrow [P_5X_2]^+[Al(OR)_4]^-, \mathbf{4a,b} + AgX \quad (5)$$
$$R = C(CF_3)_3 \qquad X = I: \mathbf{4a}, X = Br: \mathbf{4b}$$

In situ ^{31}P NMR spectroscopy at −80 °C showed that $P_5X_2^+[Al(OR)_4]^-$ (**4a**,**b**) was the only P-containing product visible after 10 days' reaction time. A larger preparation gave temperature-, air-, and moisture-sensitive crystalline **4b** in almost quantitative yield. Solid **4b** is stable for at least two months at −30 °C. Compound **4a** was earlier synthesized and characterized by Raman, NMR, and elemental analysis in an alternative procedure[4, 14] by treating $[Ag(P_4)_2]^+[Al(OR)_4]^-$ in CD_2Cl_2 with 3.5 equivalents of I_2 at −78 °C.

When P_2I_4 was treated with $Ag[Al(OR)_4]$ [Eq. (6)] in CS_2/CH_2Cl_2 (90:10) at RT, an initially formed, highly electrophilic cation ($P_2I_3^+$?) decomposed the anion, and $[P_2I_5(CS_2)]^+$ $[(RO)_3Al\text{-}F\text{-}Al(OR)_3]^-$ **5** was formed as the main soluble product, crystallizing in 70% yield (based on Al) from the concentrated solution.

0947-6539/02/0819-4476 $ 20.00+.50/0 *Chem. Eur. J.* **2002**, *8*, No. 19

$$Ag[Al(OR)_4] + P_2I_4 \rightarrow P_2I_5(CS_2)^+[(RO)_3Al\text{-}F\text{-}Al(OR)_3]^-, \mathbf{5} + AgI\ (+\,?)$$
$$R = C(CF_3)_3 \qquad (6)$$

This is the third example of the fluoride-bridged $(RO)_3Al\text{-}F\text{-}Al(OR)_3^-$ anion, which appears to be a general decomposition product of the $Al(OR)_4^-$ anion. An in situ NMR reaction according to Equation (6) that was always kept at temperatures below $-30\,^\circ C$ showed that the initially produced cation ($P_2I_3^+$?) is not stable under these conditions, and that $P_2I_5^+$ (80%) and $P_3I_6^+$ (20%) were the only P-containing decomposition products visible in the ^{31}P NMR spectrum at $-80\,^\circ C$.

Crystal structures: Details on the crystal structure solution and refinement are included in Table 15 below. The (normal) geometries of the $Al(OR)_4^-$ anions and the solid state packing of the salts are included and discussed in a deposited section.

*The PX_4^+ cations in **1a**,**b***: Figure 1 provides views of the S_4-symmetric PX_4^+ cations in **1a**,**b**. Full ellipsoid plots including the anion have been deposited. The (only) short P–I (P–Br) bond length is 2.3700(4) (2.1106(9)) Å and is about 0.03

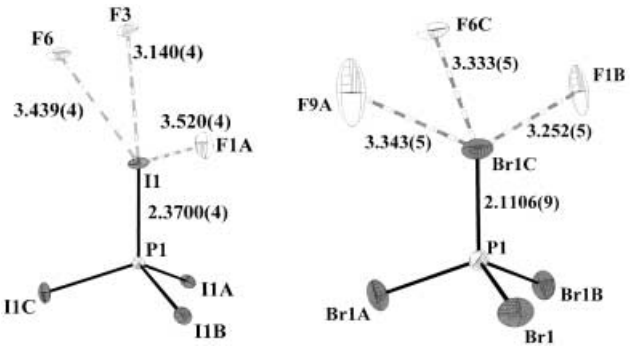

Figure 1. Geometry and one set of X–F contacts (X = Br, I) of the S_4-symmetric PX_4^+ cations in **1a**,**b**. The other X–F contacts are symmetry-equivalent and, therefore, not shown. Anisotropic thermal ellipsoids were drawn at the 25% probability level, the P–X bond lengths [Å] are given within the figure. The I-P-I (Br-P-Br) bond angles range from 109.2(1) to 109.6(1)° (109.3(1) to 109.9(1)°).

(0.02–0.06) Å shorter than those found in PI_4AlI_4 ($PBr_4^+Br^-$), which is best described as a network of strongly interacting PI_4^+ (PBr_4^+) cations and AlI_4^- (Br^-) anions with I–I contacts as short as 3.386 Å.[16, 17] However, the P–I bond length compares well with that for the recently published more ionic $PI_4^+AlCl_4^-$ [$d(P\text{–}I)_{av.} = 2.368(4)$ Å].[1b] The PX_4^+ cations, which are only very slightly distorted from T_d symmetry, are bisphenoidally elongated (cf. the I-P-I (Br-P-Br) bond angles range from 109.2(1) to 109.6(1)° (109.3(1) to 109.9(1)°)) and are stabilized by four sets of symmetry-equivalent weak X–F contacts at 3.140(4), 3.439(4), and 3.520(4) Å (**1a**) or 3.252(5), 3.333(5), and 3.343(5) Å (**1b**), which are shorter than the sum of the F and X van der Waals radii of 3.60 (I) or 3.40 Å (Br) (Figure 1). In contrast to $AsCl_4^+$,[18] no E–F contacts (E = P, As) below 4.276 (**1a**) or 4.047 Å (**1b**) were observed.

*The $P_2X_5^+$ salts **3a**,**b***: Both salts form a fourfold twinned 200 K phase. The unit cell of **3a**,**b** appeared to be tetragonal with lattice constants that are similar to but slightly larger than those of the salts $PX_4^+[Al(OR)_4]^-$ (**1a**,**b**) (Table 1).

Table 1. Lattice constants and volume of the tetragonal $PX_4^+[Al(OR)_4]^-$ **1a**,**b** salts and those of the fourfold twinned $P_2X_5^+[Al(OR)_4]^-$ **3a**,**b** salts at 200 K.

Parameter	**1a** (150 K)	**3a** (200 K)	**1b** (200 K)	**3b** (200 K)
$a = b$ [Å]	13.978(2)	14.510(3)	13.640(2)	14.016(3)
c [Å]	9.4045(19)	9.778(2)	9.449(2)	9.694(2)
V [Å^3]	1837.4(5)	2058.6(7)	1758.0(5)	1904.3(7)

The PX_4^+ and $P_2X_5^+$ cations reside on similar positions; however, since the $P_2X_5^+$ cation only has a local C_s symmetry, it is clear that it is impossible for the cation to reside on a special position with local S_4 symmetry without fourfold twinning. As evident from the triclinic solution of the crystal structure, which provided a disordered view of the cation, the twinning element was a fourfold axis parallel to c. By including this twinning law and lowering the symmetry from tetragonal to triclinic, the structures could be solved and refined to final $R1$- (w$R2$-) values of 0.0670 (0.1722) for **3a** and 0.0712 (0.1678) for **3b**. The four domains of the fourfold twins were populated by 22 to 28%. However, as evident from the difference Fourier maps of the refined twinned structure, the $P_2X_5^+$ cations were also disordered over two positions in a 80:20 ratio (figure deposited). Due to the disorder, the standard deviations of the structural parameters of the cations are larger, and the solid-state structures are mainly seen as structural proof for the existence of the $P_2X_5^+$ and the intact $Al(OR)_4^-$ ions. Structural data for the cations of **3a**,**b** are included in Table 13 below. Views of the asymmetric unit of **3a**,**b** at 200 K have been deposited. When **3b** was crystallized at $-80\,^\circ C$, and the crystals were measured at 150 K, a truly triclinic phase with similar lattice constants to the 200 K phase was obtained ($a = 9.829(2)$ Å, $b = 13.702(3)$ Å, $c = 13.906(3)$ Å, $\alpha = 90.79(3)^\circ$, $\beta = 94.08(3)^\circ$, $\gamma = 90.31(3)^\circ$, $V = 1867.9(6)$ Å^3). No disorder was evident in this structure, and consequently the standard deviations are smaller (Figure 2).

The geometry of the $P_2Br_5^+$ cation of **3b** is similar to that of the $P_2I_5^+$ cation with a very small increase in the P–P bond length of at most 0.026 Å. Two distinct sets of P–Br distances are found: longer P–Br separations of 2.184(3) and 2.199(3) Å in the $P^{II}Br_2$ moiety and shorter P–Br bond lengths of 2.115(2) to 2.129(2) Å in the $P^{IV}Br_3$ phosphonium unit. Complete structural parameters and a discussion of the geometry are given below (Table 13).

*The $P_2I_5^+$ salt **5***: Long, thin, yellow needles of **5** (dimensions up to $20 \times 0.5 \times 0.3$ mm) grew from a solution in CS_2/CH_2Cl_2 (90:10) at $-30\,^\circ C$ and were found to be triclinic, space group $P\bar{1}$ with two molecules in the unit cell. We recorded several complete data sets of these crystals at 170 K and 150 K, but in all cases the $P_2I_5^+$ cation in **5** resides on two independent positions in a 85:15 or 20:80 ratio (see Figure 3).

In crystal **5**′, 85% of the $P_2I_5^+$ cations coordinated more strongly to an incorporated CS_2 molecule (d(P2–S2) = 3.215 Å), and in another crystal **5**″ of the same batch, 80% of the cations were well separated from the CS_2 molecule (d(P2–S2) > 4.0 Å). The CS_2 coordination greatly influenced

  0947-6539/02/0819-4477 $ 20.00+.50/0

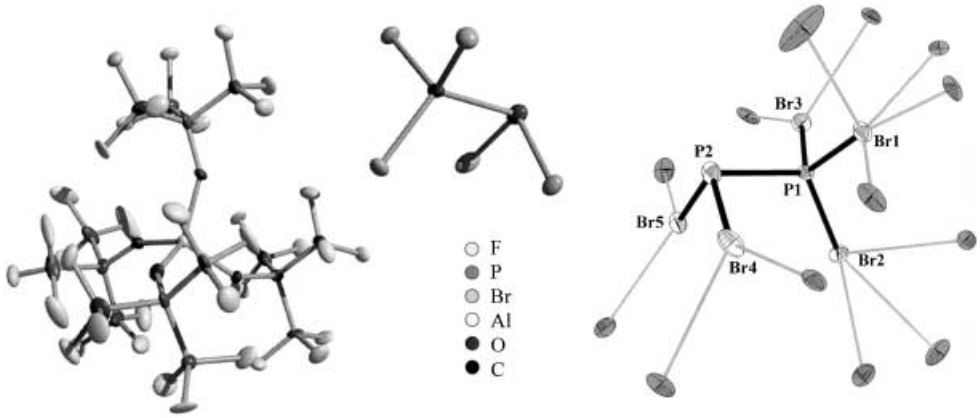

Figure 2. Left: Solid-state structure of the salt $[P_2Br_5]^+[Al(OR)_4]^-$ **3b** at 150 K. Right: Geometry and E–F contacts (E = Br, P) of the $P_2X_5^+$ cations in **3b**. The bonds within the $P_2Br_5^+$ cation are drawn black and bold, those to the fluorine atoms gray and thin. The 13 Br–F contacts range from 3.172(7) to 3.362(7) Å, and the structural parameters of the $P_2Br_5^+$ cation are included in Table 13. Anisotropic thermal ellipsoids were drawn at the 25% probability level.

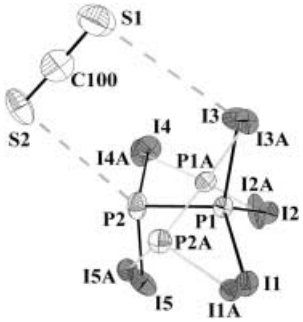

Figure 3. The two independent positions of the $P_2I_5^+$ cation in **5′**. Atoms P1 to I5 have a 85% occupancy (black bonds) and P1A to I5A have a 15% occupancy (gray bonds). A similar situation was observed in **5″**; however, the occupancy factors were inverted (20:80).

the geometries of the two $P_2I_5^+$ cations in **5**, therefore both are described.

The $P_2I_5(CS_2)^+$ cation in **5′**: Figure 4 shows that 85% of $P_2I_5^+$ cations coordinate one CS_2 molecule via a stronger P2–S2 (3.215(6) Å) and a weak I3–S1 (4.072(4) Å) interaction (sum of the P–S and S–I van der Waals radii: 3.75 and 4.00 Å). The overall geometry of the staggered $P_2I_5^+$ cation with slightly longer P–I separations in the PI_2 unit is similar to that found in $P_2I_5AlI_4$; however, differences appear when the P–I bond lengths are studied in more detail. In **5′** they are found between 2.348(4) and 2.542(4) Å, which may be compared to 2.399(9) to 2.420(9) Å in $P_2I_5AlI_4$. This is attributed to the coordination of the CS_2 molecule. The S2 lone-pair orbital presumably donates electron density into the antibonding σ* orbital of the P2–I5 bond and consequently elongates this bond by about 0.1 Å (see Figure 4 for a drawing of the suitable orientation of CS_2 and $P_2I_5^+$). Charge transfer from the (formally) unipositive phosphonium center P1 to the other atoms must have occurred, as evidenced by the formation of one P–S, two I–S, and five I–F contacts (see Figure 4).

The $P_2I_5^+$ cation in **5″**: 80% of $P_2I_5^+$ cations in **5″** are well separated from the incorporated CS_2 molecule, therefore the P–I bond lengths in this species are in the narrower range of 2.369 to 2.460 Å. All other structural parameters are com-

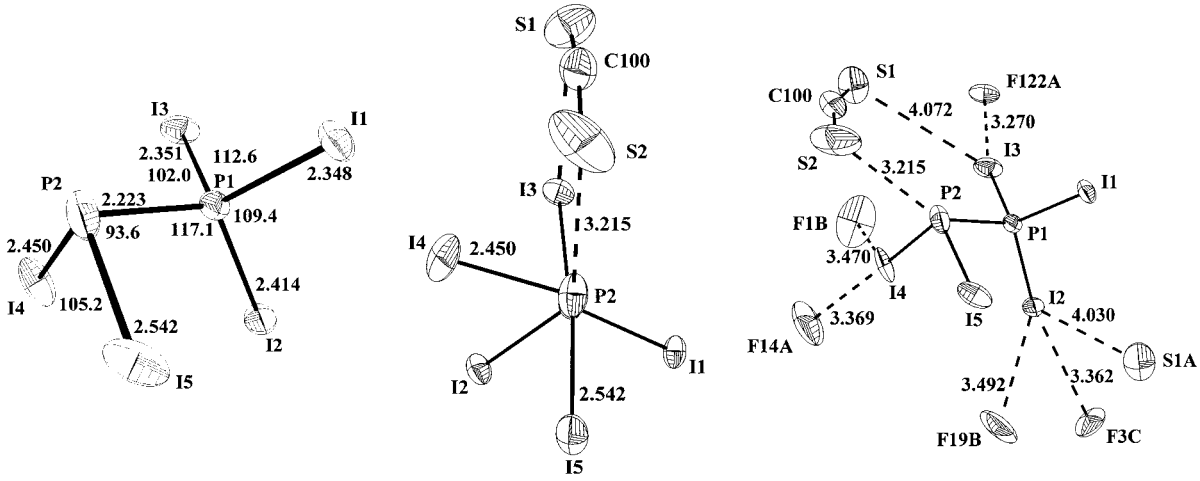

Figure 4. Geometry of the $P_2I_5(CS_2)^+$ cation in $[P_2I_5(CS_2)]^+[(RO)_3Al\text{-}F\text{-}Al(OR)_3]^-$, **5′**. Anisotropic thermal ellipsoids were drawn at the 25% probability level, selected bond lengths [Å] and bond angles [°] are given in the figure, standard deviations are 0.004 Å for P–I and P–P bond lengths and 0.2° for the bond angles.

0947-6539/02/0819-4478 $ 20.00+.50/0 *Chem. Eur. J.* **2002**, *8*, No. 19

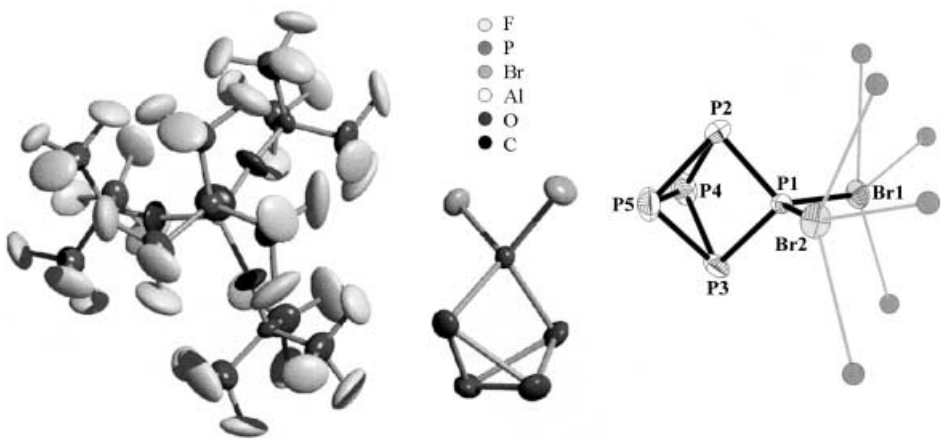

Figure 5. Left: The solid-state structure of **4b** at 200 K (25% ellipsoids). Right: The structure and Br–F contacts of the $P_5Br_2^+$ cation in **4b** at 200 K (25% ellipsoids). The six Br–F contacts range from 3.025 to 3.380 Å, no P–F contacts below 3.411 Å were observed (sum of P and F van der Waals radii: 3.40 Å). Structural parameters of the cation are included in Table 14.

parable to those of **5′**, **3a**, or $P_2I_5AlI_4$ (structural parameters in Table 13 below; figure deposited).

*The $P_5Br_2^+$ cation in **4b***: The crystal structure determination[19] of a colorless monoclinic block of **4b** confirmed the nature of the almost C_{2v}-symmetric $P_5Br_2^+$ cation (Figure 5) and the presence of the intact $Al(OR)_4^-$ anion.

This P_5 cage is without precedence and was not found as part of the many polyphosphides or organopolyphosphanes known to date.[20, 21] The range of the P–P bond lengths in the $P_5Br_2^+$ cation of 2.150(7) to 2.262(8) Å is close to the values found in P_4 (2.21 Å) or $Ag(P_4)_2^+$ (2.15–2.32 Å).[10] The P–P bonds to the tetracoordinate PX_2 phosphonium atom are shorter than those to the remaining naked P atoms by about 0.06 to 0.08 Å.

The $(RO)_3Al$-F-$Al(OR)_3^-$ anion: The fluoride-bridged anion was earlier found in two salts[4] and now in **5**. It consists of a linear central Al-F-Al unit (d(Al–F) = 1.758–1.775 Å). Each Al atom is additionally coordinated by three OR ligands with very short Al–O bond lengths of 1.673 to 1.698 Å. The anions are staggered with respect to the orientation of the two AlO_3 units, and the central fluorine atoms reside on centers of inversion (see Figure 6 and Table 2).

The average Al–O bond lengths (Al-O-C bond angles) in the fluoride bridged anions are shorter (wider) than those of the homoleptic $Al(OR)_4^-$ anion; this accounts for the greater electron deficiency of the aluminum centers in the $(RO)_3Al$-F-$Al(OR)_3^-$ anion. Based on the structural parameters and the space filling model,[4] it is evident that the $(RO)_3Al$-F-$Al(OR)_3^-$ anion with 54 peripheral C–F bonds is more stable against RO^- abstraction and less coordinating than the homoleptic $Al(OR)_4^-$ anion, with 36 peripheral C–F bonds.[4] The $(RO)_3Al$-F-$Al(OR)_3^-$ anion is probably the least coordinating anion currently known.

Assignment of thermochemical volumes to the P–X cations: The thermochemical volume of the $Al(OR)_4^-$ anion was established as 758 Å^3.[22] This knowledge then allowed the thermochemical volumes of the P–X cations to be established from the unit cell volumes of the salts (Table 15 below). By using Jenkins' volume-based lattice-energy equation,[23] the lattice potential energies of the salts were calculated and are collected with the thermochemical volumes in Table 3.

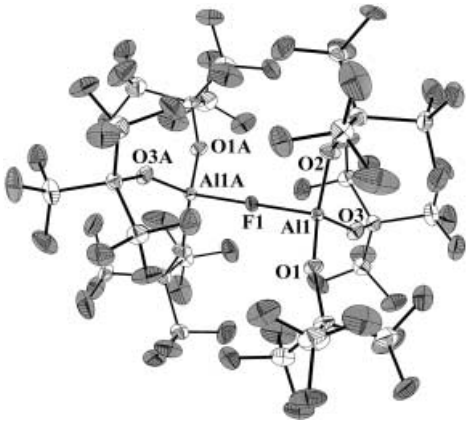

Figure 6. Structure of the $(RO)_3Al$-F-$Al(OR)_3^-$ anion in **5**. The oxygen (light gray), aluminum (white), fluorine (dark gray), and carbon atoms (white) were drawn with anisotropic thermal ellipsoids at the 25% probability level.

Due to the large size of the anion, the lattice potential energies of all prepared salts are very low and are already close to the "lattice enthalpies" of molecular solids of comparable atomic weight, such as C_{60} (M_r = 720) or C_{70} (M_r = 840), for which sublimation enthalpies of 175 and 200 kJ mol^{-1} were reported [cf. M_r(**1b**) is 1318 and higher than the molecular weight of any substance for which a sublimation enthalpy is tabulated[7]). This adds further evidence to our previous notion that large

Table 2. Comparison of the structural parameters of the $(RO)_3Al$-F-$Al(OR)_3^-$ anions in **5** and $[P_3I_6]^+[(RO)_3Al$-F-$Al(OR)_3]^-$.[4] Typical data of the $Al(OR)_4^-$ anion are given for comparison ($Ag(Cl_2C_2H_4)_3^+$ salt).[9]

Parameter	Al-F-Al[a]	**5′**	**5″**	$Al(OR)_4^-$[9]
d(Al-O) range [Å]	1.671(9)–1.700(9)	1.673(6)–1.698(5)	1.681(6)–1.694(5)	1.714(3)–1.736(3)
$d(\text{Al-O})_{av.}$ [Å]	1.687	1.685	1.689	1.725
$(\text{Al-O-C})_{av}$ [°]	154.9	156.1	153.1	149.5
d(Al-F) range [Å]	1.760(4)–1.761(4)	1.758(2)–1.770(2)	1.764(2)–1.775(2)	–
$d(\text{Al-F})_{av}$ [Å]	1.761	1.764	1.770	–
(Al-F-Al) [°]	180	180	180	–

[a] The $(RO)_3Al$-F-$Al(OR)_3^-$ anion in $P_3I_6^+[(RO)_3Al$-F-$Al(OR)_3]^-$.[4]

Table 3. Thermochemical volumes V_{th} [Å^3] and estimated Lattice potential energies U_L[23] of the binary P–X cations [kJ mol^{-1}].

Halide	$V_{th}(PX_4^+)$	$U_L(PX_4Al)$[a]	$V_{th}(P_2X_5^+)$	$U_L(P_2X_5Al)$[a]	$V_{th}(P_5X_2^+)$	$U_L(P_5X_2Al)$[a]
X = I	161	345	271	336	–	–
X = Br	121	349	194	342	180	343

[a] Al = Al(OR)$_4$.

and weakly coordinating anions produce *"Pseudo Gas-Phase Conditions"* in condensed phases.[24, 25]

Computational chemistry: To understand the bonding and the thermodynamics of the formation of the binary P–X cations, several binary P–X compounds, AgBr, Ag^+, Br^-, and Br_2, were optimized at the (RI-)MP2/TZVPP level, which we showed earlier[4] to be the most suitable level of theory to economically assess the geometries and the thermodynamics of the species in question. The data of P_4 (T_d), $P_5I_2^+$ (C_{2v}), $P_3I_6^+$ (C_2), $P_2I_5^+$ (C_s), P_2I_4 (C_{2h}), PI_3 (C_s), PI_2^+ (C_{2v}), I_2, AgI, and Ag^+ were taken from earlier work;[4, 14] only $P_2I_3^+$ (C_s), PI_4^+ (T_d), PBr_4^+ (T_d), PBr_3 (C_{3v}), PBr_2^+ (C_{2v}), $P_5Br_2^+$ (C_{2v}), and $P_2Br_5^+$ (C_s) were newly optimized (see Figure 7 and deposited table).

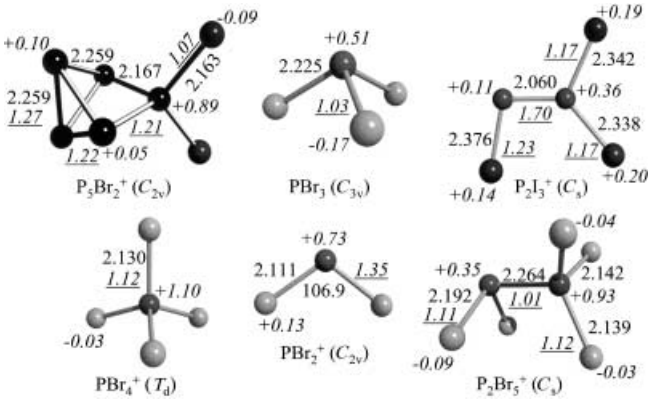

Figure 7. (RI-)MP2/TZVPP geometries of $P_2I_3^+$ (C_s), PBr_4^+ (T_d), PBr_3 (C_{3v}), PBr_2^+ (C_{2v}), $P_5Br_2^+$ (C_{2v}), and $P_2Br_5^+$ (C_s). Computed partial charges are given in italics, shared electron numbers (*SEN*) in italics and underlined. All species included are true minima with no imaginary frequencies.

Comparison of the computed P–X distances of 2.225 or 2.451 Å (PX_3) and 2.130 or 2.373 Å (PX_4^+) to the experimental PX_3 and PX_4^+ geometries with d(P–X) = 2.22 or 2.43 Å (PX_3) and 2.1106(9) or 2.3700(4) Å (PX_4^+) establishes the quality of the MP2 calculation. In contrast, earlier calculations[18, 36] on the PX_4^+ cations gave an overestimation of the P–X bond lengths of about 0.05 Å. Also the difficult to model[4] $P_2X_5^+$ geometries with an experimental d(P–P) of 2.22(1) to 2.246(3) Å were reproduced by MP2 to within 0.02 Å, while BP86 and B3LYP optimizations overestimated the P–P distance by 0.10 to 0.19 Å.[4] The calculated $P_2I_3^+$ geometry is rather remarkable – the ion contains what is almost a P=P double bond [*SEN*(P–P) = 1.70] and extensive charge delocalization, which leads to short P–I bonds with high shared electron numbers *SEN*(P–I). When comparing the computed partial charges of all P–I[4] against the P–Br species, one notes that the partial charges of the species bearing the less electronegative iodine ligand are considerably more delocalized than those of the species with the more electronegative bromine ligand (Figure 7). This shows most strongly for the tetracoordinate phosphonium centers in PX_4^+, $P_2X_5^+$, and $P_5X_2^+$. For X = I, the partial charges of the tetracoordinate phosphorus atoms are +0.48, +0.47, and +0.57, but for X = Br the charges increase to +1.10, +0.93, and +0.89. However, the *SEN*s of the P–P and P–X bonds of the homologous species are nearly unchanged and similar to within 0.04.

Enthalpies of formation of the P–X cations: The enthalpies of formation of gaseous PBr_2^+,[45, 53] P_4,[7] Br_2,[7] I_2,[7] and PBr_3[45, 53] at 298 K were determined as +862, +54, +31, and −91 kJ mol^{-1}. Those of PI_2^+ and PI_3 were derived[26] as +919 and +52 kJ mol^{-1}. With these and the calculated reaction enthalpies in Table 11 below, the enthalpies of formation of the gaseous P–X cations were assessed at 298 K.[27, 28]). The $P_2I_5^+$ and $P_5I_2^+$ values of 749 and 784 kJ mol^{-1} in Table 4 are in good agreement with our earlier,[4] independently derived values of 733 ($P_2I_5^+$) and 792 kJ mol^{-1} ($P_5I_2^+$).

Table 4. Derived enthalpies of formation of the gaseous P–X cations at 298 K.

Halide	$\Delta_f H(PX_4^+)$	$\Delta_f H(P_2X_5^+)$	$\Delta_f H(P_5X_2^+)$
X = Br	+617 kJ mol^{-1}[27a]	+579 kJ mol^{-1}[27b]	+705 kJ mol^{-1}[27c]
X = I	+764 kJ mol^{-1}[28a]	+749 kJ mol^{-1}[28b]	+784 kJ mol^{-1}[28c]

Raman and IR spectra of the P–X cations, calculated bands of PX_4^+, $P_2X_5^+$, and $P_5X_2^+$: The PI_4^+ and $P_2I_5^+$ cations are very sensitive to the IR laser (1064 nm) and decompose easily in the beam. We only succeeded in obtaining a reasonable[29] room-temperature Raman spectrum of **1a** and **5** when large single crystals (at least 0.5 × 0.5 × 0.5 mm) were sealed in a NMR tube. Smaller crystals, powders, and ground material of **1a** and **3a** decomposed much faster and never gave a spectrum of sufficient quality, even if low laser power and wide focus were used. In spectra of these samples of **1a**, we only observed a weak iodine band at 180 cm^{-1}. All P–Br cations and $P_5I_2^+$ are less sensitive toward the laser beam, and we succeeded in obtaining their Raman and/or IR spectra. The vibrational spectra of the anions in **1a**,**b**, **3a**,**b**, and **4a**,**b** are deposited (Supporting Information, Tables 3 and 4).

PX_4^+ vibrations: The bands of the PBr_4^+ salts **1a**,**b** are collected and assigned in Table 5. The positions of the bands in **1a**,**b** are in good agreement with the calculations and the experimental spectra of $PBr_4^+AsF_6^-$ and $PI_4^+AlCl_4^-$.[1b] However, more basic anions such as AlX_4^- and GaX_4^- (X = Br, I) shifted all bands to lower energy by about 10 – 20 cm^{-1} due to cation – anion interactions.[1b] It may be noted that three

0947-6539/02/0819-4480 $ 20.00+.50/0 *Chem. Eur. J.* **2002**, *8*, No. 19

Table 5. Experimental vibrational wavenumbers of **1b** and $PBr_4^+AsF_6^-$,[1b] calculated wavenumbers of PBr_4^+ (MP2/TZVPP).

PBr_4^+ Calcd (sy) (IR:%)	**1b** IR (Int.)	**1b** RA (%)	$PBr_4^+AsF_6^-$ IR (Int.)[1b]	$PBr_4^+AsF_6^-$ RA (%)[1b]	PI_4^+ calcd (sy) (IR:%)	**1a** IR (Int.)	**1a** RA (%)	$PI_4^+AlCl_4^-$ IR[1b]	$PI_4^+AlCl_4^-$ RA[1b]	Assignment
528 (T_2) (100)	514 (vs)	–	513 (s)	512 (8)	437 (T_2) (100)	400 (vs)	406 (w)	399 (s)	400 (17) 394 (17)	$\tilde{\nu}$ P–X
270 (A_1) (0)	–	265 (100)	–	266 (100)	187 (A_1) (0)	–	175 (100)	–	169 (100)	Breathing mode
155 (T_2) (0)	–	152 (88)	–	153 (66)	104 (T_2) (0)	–	–	–	98 (25)	PX_3 deformation
101 (E) (0)	–	–	–	106 (34)	68 (E) (0)	–	–	–		PX_4 torsion

different values of the most intense symmetric A_1 mode were reported for $PI_4^+AsF_6^-$: 193 cm^{-1},[6] 180 cm^{-1},[30a, 36] and 178 cm^{-1}.[30b] The first value appears to be very high in energy since $PI_4^+AlCl_4^-$, with a rather short P–I distance of 2.368(4) Å, shows this band at 169 cm^{-1}; **1a**, including a less-basic anion than AsF_6^-, is found at 175 cm^{-1}. The second and third reported values of 180 and 178 cm^{-1} are at the positions where solid iodine is found (180 ± 2 cm^{-1}). With the usual accuracy of the Raman spectrometer of 2–4 cm^{-1}, we therefore suggest that the assignment of the two bands at 178 or 180 cm^{-1} being the A_1 mode of PI_4^+ may possibly be wrong and be due rather to decomposition and formation of I_2.

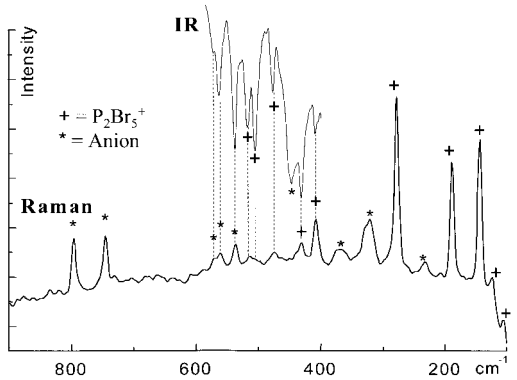

Figure 8. Vibrational spectra of the new $P_2Br_5^+$ cation in **3b**.

$P_2X_5^+$ vibrations: Figure 8 and Table 6 include the vibrational spectra and assignments of the bands of the $P_2X_5^+$ salts **3a**,**b** and **5**. The actual spectra of **3a** and **5** have been deposited. The Raman samples of **3a** always decomposed in the laser beam and therefore showed bands due to decomposition (P_2I_4); however, the five most intense bands of **3a** at 328, 223, 137, 105, and 87 cm^{-1} are in good agreement with those observed for **5** containing the more stable[4] $(RO)_3Al\text{-}F\text{-}Al(OR)_3^-$ anion or $P_2I_5AlI_4$ (Table 6). The high-energy bands of **3a** were also observed in the IR spectrum. The vibrational bands of the hitherto unknown $P_2Br_5^+$ cation in **3b** shown in Figure 8 are related to those of the $P_2I_5^+$ cation. All modes of $P_2Br_5^+$ are found at higher energy by 40 to 70 cm^{-1} than those of the $P_2I_5^+$ cation, and 11 out of the 15 expected fundamental vibrational bands were observed.

The vibrational spectra of **3a** and **5** are very similar, the observed bands represent the vibrations of an almost "naked" $P_2I_5^+$ cation, and all vibrations of $P_2I_5AlI_4$ are at lower energy than the respective bands in **3a** or **5** due to the strongly interacting $P_2I_5^+$ and AlI_4^- ions.[31] The Raman spectra of the $P_2I_5EI_4$ (E = Al, Ga, In) series of compounds were recently assigned based on a B3LYP optimization and frequency calculation of the $P_2I_5^+$ cation.[3, 32] This B3LYP optimization[3] failed considerably to reproduce the experimental geometry (i.e., the optimized P–P bond length was 2.366 Å vs. 2.218 Å found in $P_2I_5AlI_4$ or 2.223 Å in **5**; see ref. [4] for a comment on the calculation). The highest calculated vibrational wavenumber of this $P_2I_5^+$ was reported at 394 cm^{-1}. Since in (the similar) P_2I_4 a Raman band at 443 cm^{-1} (14% relative intensity, P–P stretch) is observed, it appeared surprising that no band at a higher energy than 394 cm^{-1} was calculated (and no band above 390 cm^{-1} was assigned in the experimental

Table 6. Experimental vibrational wavenumbers of **3a**, **3b**, **5**, and $P_2I_5AlI_4$; calculated wavenumbers of $P_2X_5^+$ (X = Br, I; MP2/TZVPP).

$P_2I_5^+$ calcd (sy) [IR:%]	**3a** IR	**3a**[a] RA	**5** exp. [%]	$P_2I_5AlI_4$[3] exp. [%]	$P_2Br_5^+$ calcd (sy) [IR:%]	**3b** IR (Int.)	**3b** RA [%]	Assignment
462 (a′) (59)	430 (sh)	–	(430?)	430[b]	528 (a′) (65)	517 (s)	515 (3)	$\tilde{\nu}$ P–P, $\tilde{\nu}_{as}$ PX_3
437 (a″) (100)	413 (s)	–	409 (6)	390 (10)	517 (a″) (100)	504 (s)	n.o.[c]	$\tilde{\nu}_{as}$ PX_2 of PX_3 unit
420 (a′) (66)	401 (s)	–	398 (6)	384 (20)	483 (a′) (34)	475 (m)	475 (4)	$\tilde{\nu}$ P–P, $\tilde{\nu}_s$ PX_3
389 (a″) (63)	364 (s)	–	363 (10)	348 (5)	442 (a″) (44)	430 (m)	431 (9)	$\tilde{\nu}_{as}$ PX_2
354 (a′) (23)	330 (s)	328	331 (57)	324 (10)	418 (a′) (16)	408 (w)	408 (24)	$\tilde{\nu}_s$ PX_2
235 (a′) (23)	223 (m)	223	223 (84)	210 (100)	287 (a′) (25)	278 (w)	279 (100)	PX_3P breathing mode[d]
142 (a′) (2)	–	137	136 (100)	129 (60)	192 (a′) (4)		189 (69)	δ_s trans P_2X_4 unit
107 (a″) (0)	–	–	in 104?	in 97?	147 (a″) (0)		in 144?	δ_{as} PX_3
105 (a′) (1)	–	105	104 (10)	97 (40)	146 (a′) (2)		144 (86)	δ_s PX_2
88 (a′) (0)[e]	–	87	86 (6)	89 (20)	127 (a′) (0)		124 (6)	δ_s trans-P_2X_4 unit
–	–	-	–	–	102 (a″) (0)[f]		102 (6)	δ_{as} PX_3

[a] Compound **3a** decomposed rapidly in the Laser beam of the Raman spectrometer with formation of P_2I_4, and therefore only the five most intense bands, which were unambiguously assigned, are given. [b] In the depicted spectrum in Ref. [3] a very weak and unassigned band at about 430 cm^{-1} is visible in all three spectra of $P_2I_5EI_4$ (E = Al, Ga, In). [c] Not observed. [d] Breathing mode of the ligands of the tetrahedrally coordinated P atom. [e] Calculated low-frequency bands: 74 (a″) (0), 69 (a′) (0), 53 (a′) (0), 47 (a″) (0), 27 (a′) (0). [f] Calculated low-frequency bands: 89 (a′) (0), 69 (a′) (0), 59 (a″) (0), 38 (a′) (0).

  0947-6539/02/0819-4481 $ 20.00+.50/0

spectrum).[3] We suggest that this is due to overestimation of the P–P bond length of the $P_2I_5^+$ cation at the B3LYP level (0.14 to 0.15 Å too long). Our MP2/TZVPP frequencies of the $P_2I_5^+$ cation with a P–P separation only overestimated by 0.01 to 0.03 Å showed the highest two (unscaled) bands at 462 and 437 cm^{-1}. With the knowledge of an expected band above 400 cm^{-1}, we reinspected the Raman spectra depicted in ref. [3] and, indeed, very weak bands around 430 cm^{-1} are visible in all three spectra of $P_2I_5EI_4$ (E = Al, Ga, In). Also the IR spectrum of **3a** has a shoulder at 430 cm^{-1}.[33] Therefore we propose that the assignments of the vibrations ω_1 to ω_4 given in ref. [3] are wrong. Due to the insufficient quality of the optimized geometry of $P_2I_5^+$ in ref. [3], all calculated bands appeared at lower energy and, therefore, the very weak highest energy P–P stretching bands at approximately 430 cm^{-1} (exp.) were overlooked.[34]

$P_5X_2^+$ vibrations: Raman spectroscopy showed that also the bulk material is pure **4a**,**b**. Observed and calculated vibrational wavenumbers of the $P_5X_2^+$ cations are collected in Table 7, and the actual spectra have been deposited. Ten (**4a**) and 13 (**4b**) out of the 15 expected vibrational bands of the cations were observed, and all bands of the P_5 cage are strongly mixed. The symmetric breathing mode of the P_5 cage (A_1, **4a**: 541, **4b**: 553 cm^{-1}) is slightly weakened compared with the A_1 mode of P_4 (600 cm^{-1}) but higher in energy than the P–P vibrations of red phosphorus (highest energy band at 461 cm^{-1}).[35]

Variable-temperature ^{31}P NMR spectroscopy of the P–X cations: All ^{31}P NMR shifts assigned to the P–X cations are collected in Table 10 below and compared to known shifts. One comment prior to discussion: It is not adequate to calculate the ^{31}P NMR chemical shifts of the P–X cations by the standard procedures built into many quantum chemical program codes due to relativistic spin–orbit effects. Iodine, and to a lesser extent also bromine, substituents at a tetracoordinate phosphorus atom lead to a very pronounced relativistic upfield shift that may reach several hundred ppm.[36]

^{31}P NMR of PX_4^+: The room temperature ^{31}P NMR spectrum of crystalline **1a** dissolved in CD_2Cl_2 showed one broad line at $\delta(^{31}P) = -475$ that was considerably sharpened when the compound was cooled to 223 or 183 K. However, small impurities, that is a small excess of PI_3 as present in the NMR-scale reaction of 1.18 PI_3, 1.02 I_2, and 1.00 $Ag[Al(OR)_4]$ in CD_2Cl_2 (≈0.1 M), led to a fourfold increase in the half width of the signal and a worse signal-to-noise ratio than that in the less-concentrated solution of crystalline **1a** in CD_2Cl_2 (≈0.02 M; figure deposited). The line width at half height of the sample prepared from crystalline **1a** was 330 Hz, and that of the in situ reaction was 1370 Hz. The solid state ^{31}P MAS NMR shift of $PI_4^+EF_6^-$ (E = As, Sb) of $\delta = -517$ to -519 ppm[36] is in good agreement with our solution value of $\delta = -475$ ppm for **1a**. The small low-field shift ($\Delta\delta \approx$ 43 ppm) presumably originates from solvent–cation interactions, which may be seen in analogy to the strong solid-state I–I contacts in PI_4AlI_4, for which a solid-state ^{31}P MAS NMR shift of only -304 ppm was observed ($\Delta\delta \approx 214$ ppm).[36] The reason for the extreme upfield shift of the PI_4^+ cation of about 700 ppm was shown to be due to spin–orbit coupling in an external field mediated by an very efficient Fermi contact mechanism.[36]

Compound **1b** is considerably less soluble than **1a**, and ^{31}P NMR spectra of a reasonable resolution could only be obtained at +10 °C; they showed the PBr_4^+ cation to have a sharp resonance at $\delta(^{31}P) = -83$. The PBr_4^+ shift in **1b** is less affected by relativistic spin–orbit effects; however, it is still at higher field than expected by more than 200 ppm[36] and is in good agreement with the solid-state MAS NMR shift of $PBr_4^+AsF_6^-$ at -83 ppm.[1b]

^{31}P NMR spectroscopy and disproportionation of $P_2I_5^+$: The $P_2I_5^+$ cation in $P_2I_5AlI_4$ is only stable in the solid state, and NMR spectra of CS_2 solutions of the salt only furnished the signals of PI_3 and AlI_3.[3] The solid-state ^{31}P MAS NMR spectrum of $P_2I_5AlI_4$ showed two broad resonances centered at $\delta(^{31}P) = +114$ and -142; this is in good agreement with our solution values for **3a** of +126 and -156 ppm.[3] All low-temperature spectra of solutions of the $P_2I_5^+$ (P^{III}) cation of **3a** and **5** in CD_2Cl_2 showed the concentration- and time-dependent presence of subvalent $P_3I_6^+$ (= doublet (2P) and triplet

Table 7. Experimental and nonscaled calculated vibrational wavenumbers of **4a** and **4b** in cm^{-1}.

4a ν_{exp} (Int. %)	**4a** ν_{calcd}[a]	Sym.	**4b** ν_{exp} (Int. %)	**4b** ν_{calcd} (Int. %)[b]	Sym.	Assignment for **3**
541 (32)	544	A_1	553 (71)	571 (100)	A_1	ν_s, "breathing mode" of the P_5 cage
Within A_1 at 541?	537	B_1	534 (20)	557 (7)	B_1	ν_{as}, P2-P1-P3
502 (20)	505	A_1	523 (51)	538 (27)	A_1	ν_s, P_5 cage
Within B_1 at 448?	450	B_2	504 (11)	486 (4)	B_2	ν_{as}, P2,3,1 and Br1,2
448 (10)	444	B_1	443 (20)	465 (10)	B_1	ν_{as}, P2,3,4,5
385 (30)	390	B_1	387 (31)	409 (35)	B_2	ν_{as}, P_5 cage
359 (sh)	357	A_2	375 (77)	383 (34)	A_1	ν_s, P2,3,4,5
354 (80)	350	A_1	361 (37)	382 (17)	A_2	ν_{as}, P2,3,4,5
329 (70)	314	A_1	331 (29)	344 (12)	A_1	ν_s, P_5 cage
Within A_1 at 168?	170	B_1	203 (100)	203 (35)	A_1	ν_s, PBr_2 unit
168 (100)	169	A_1	191 (37)	191 (11)	B_2	ν_{as}, PBr_2 unit
126 (4)	132	B_2	150 (20)	148 (5)	B_1	P2-P1-P3 bend
87 (4)	86	A_1	120 (9)	115 (10)	A_1	PBr_2 bend
n.o.[c]	79	A_2	n.o.	84 (3)	A_2	cage deformation
n.o.	56	B_1	n.o.	60 (2)	B_2	cage deformation

[a] MP2/TZVPP frequencies. [b] MPW1PW91/6–311G(2df) frequencies. [c] Not observed.

0947-6539/02/0819-4482 $ 20.00+.50/0 *Chem. Eur. J.* **2002**, *8*, No. 19

(1P) at $\delta(^{31}P) = 91$ and -2[4, 14]). In a more concentrated (0.095 M) solution of **3a**, the amount of reduced $P_3I_6^+$ ($P^{2.33}$) grew over time to about 40 mol% after six weeks storage at $-30\,^\circ C$ (see Figure 9). In diluted solutions of crystalline **3a** or **5** (0.013 to 0.014 M), only $P_3I_6^+$ was visible after 90 days' storage at $-30\,^\circ C$ (Figure 9).

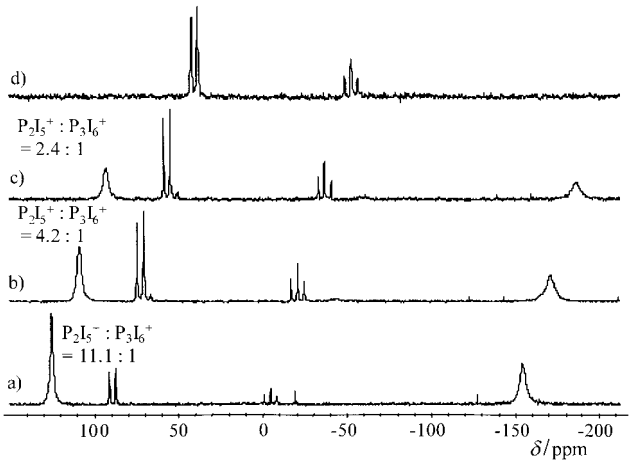

Figure 9. Solution ^{31}P NMR spectra of $[P_2I_5]^+[Al(OR)_4]^-$ (**3a**) in CD_2Cl_2 at 183 K. Time and concentration dependence of the $P_3I_6^+$ formation. a) 0.095 M solution of $[P_2I_5][Al(OR)_4]$ after 12 hours' storage at $-30\,^\circ C$; b) 0.095 M solution of $[P_2I_5][Al(OR)_4]$ after 21 days' storage at $-30\,^\circ C$; c) 0.095 M solution of $[P_2I_5][Al(OR)_4]$ after 42 days' storage at $-30\,^\circ C$; d) 0.014 M solution of $[P_2I_5][Al(OR)_4]$ after 90 days' storage at $-30\,^\circ C$.

The broad singlets of $P_2I_5^+$ with no visible P–P coupling suggest that this cation is in rapid intermolecular exchange with another species. However, although a chemical-shift range of $\delta(^{31}P) = +1200$ to -1000 ppm was scanned at several temperatures and with several independently prepared samples, no additional signal(s) apart from $P_2I_5^+$ or $P_3I_6^+$ were observed.[37] However, stoichiometry requires the formation of a more highly oxidized cation with a lower P and higher I content than $P_2I_5^+$ (P^{III}). The only known P–I cation that fulfills this prescription is PI_4^+ (P^V). Therefore the free energies ΔG of a disproportionation according to Equation (7) in Table 8 were assessed in the gas phase and in CH_2Cl_2 at $+25$, -30, and $-80\,^\circ C$ based on the MP2/TZVPP and COSMO[43] calculations. The thermal and entropic contributions to the free energy ΔG at several temperatures were calculated by Gaussian98.[44, 64]

Table 8. Free energies of dissociation of $P_2I_5^+$ at $+25$, -30, and $-80\,^\circ C$ [in kJ mol^{-1}].

Equation (7)		Temperature [°C] $+25\,^\circ C$	$-30\,^\circ C$	$-80\,^\circ C$
$2\,P_2I_5^+$ (P^{III}) $\rightarrow P_3I_6^+$ ($P^{2.33}$) + PI_4^+ (P^V)	$\Delta_r G_{gas}$	−2.63	4.23	5.71
$2\,P_2I_5^+$ (P^{III}) $\rightarrow P_3I_6^+$ ($P^{2.33}$) + PI_4^+ (P^V)	$\Delta_r G_{CH_2Cl_2}$	−5.46	1.41	2.88

An isodesmic calculation as in Equation (7) is expected to be highly accurate due to substantial error cancellation. Including the zero-point energy (ZPE), thermal corrections to the enthalpy, and entropic contributions to the free energy, Equation (7) is slightly exergonic in the gas phase and in CH_2Cl_2 at $+25\,^\circ C$. Upon cooling, entropy slightly favors the $P_2I_5^+$ side (by 1.41 kJ mol^{-1} at $-30\,^\circ C$). With the $\Delta G = -nRT \ln K$ relationship, an equilibrium constant K of 0.57 resulted for the storage temperature of the samples at $-30\,^\circ C$. Given the concentrations of the NMR samples of 0.095 and 0.013 mol L^{-1}, it can be shown[38] that in the less concentrated 0.013 M sample only the NMR shifts of the right hand side of Equation (7) are observed, while in the more concentrated 0.095 M sample, a slow disproportionation became evident, and both sides of the equilibrium were visible in the NMR spectrum.[38] However, PI_4^+ itself gives a clear ^{31}P NMR signal at $\delta = -475$ ppm with a half width of 330 Hz at $-50\,^\circ C$. However, we showed that by exchange processes, for example with PI_3, the signal of the PI_4^+ cation broadened by a factor of four and resulted in a bad signal-to-noise ratio. However, PI_3 is almost insoluble in CH_2Cl_2 at low temperatures and even a little dissolved PI_3 is sufficient to considerably broaden the signal. It is therefore reasonable to propose that a compound such as $P_2I_5^+$, which is highly soluble at low temperatures, in exchange with PI_4^+ should lead to a more pronounced line broadening. Therefore we propose—in agreement with the calculations and the absence of P–P coupling in the broad singlets of $P_2I_5^+$ in Figure 9—that due to exchange processes with $P_2I_5^+$, the PI_4^+ cation in Equation (7) is invisible on the timescale of NMR spectroscopy. Attempts to verify this hypothesis by solution Raman spectroscopy of a solution of **3a** in CD_2Cl_2 (0.1M) failed due to fluorescence and low intensities of the cations in question. An experimental proof of Equation (7) could therefore not be given, and the disproportionation remains an, albeit reasonable, hypothesis. Similar (reversible) disproportionation reactions are known for $[Se_6I_2]^{2+}[AsF_6]^-_2$ (**6**). Dissolution of single crystals of **6** in SO_2 reversibly gave at least 15 different cations as shown by ^{77}Se NMR spectroscopy.[39] Also the S_8^{2+} dication in $[S_8]^{2+}[AsF_6]^-_2$ (reversibly) disproportionates in SO_2 to give various sulfur cations.[40] The related and structurally similar $Sb_2Me_5^+$ cation interconverts rapidly in solution.[41]

Coalescence of $P_2I_5^+$: A room-temperature ^{31}P NMR of a freshly prepared solution of **3a** in CD_2Cl_2 showed only a broad signal at $\delta(^{31}P) = 35$ ($\tilde{\nu}_{1/2} = 1580$ Hz) that vanished upon cooling to 253 K (= coalescence temperature). Further successive cooling to 193 K again showed the two independent P nuclei in $I_2P^A–P^BI_3^+$ at $\delta(^{31}P) = 126$ (P^A) and -156 (P^B) (figure deposited). The free activation energy for the process :

$$I_2P^A–P^BI_3^+ \rightarrow I_2P^B–P^AI_3^+ \qquad \Delta G^{\neq} = 38\ kJ\,mol^{-1} \tag{8}$$

was estimated by using the Eyring equation[42] to be 38 kJ mol^{-1}.

^{31}P NMR of $P_2Br_5^+$: The $P_2Br_5^+$ cation in **3b** appears to be even more dynamic than the $P_2I_5^+$ cation. In several NMR samples of crystalline **3b** even at temperatures of $-90\,^\circ C$ only broad signals at $\delta(^{31}P) = 228$, 155, and 45 were observed (Figure 10). No further signal was visible between $+1300$ and -1000 ppm at -90, -80, -70, -50, and $-30\,^\circ C$. Already upon warming to $-50\,^\circ C$, the two signals at $\delta(^{31}P) = 228$ and

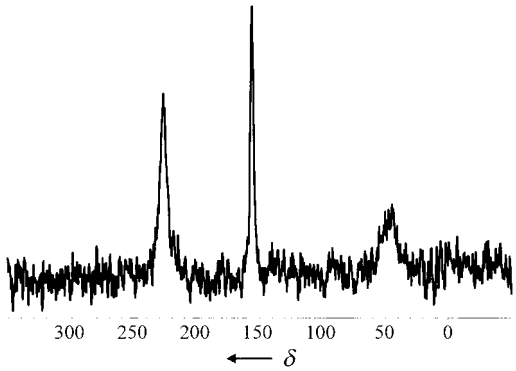

Figure 10. Solution ^{31}P NMR spectrum of crystalline $P_2Br_5^+[Al(OR)_4]^-$, **3b**, in CD_2Cl_2 at $-90\,^{\circ}C$.

45 vanished leaving the resonance at $\delta = 155$ ppm as the only remaining signal. To obtain a reliable comparison for the assignment of the ^{31}P NMR shifts of the dissolved $P_2Br_5^+$ cation, we recorded the ^{31}P MAS spectrum of solid **3b** at room temperature shown in Figure 11.

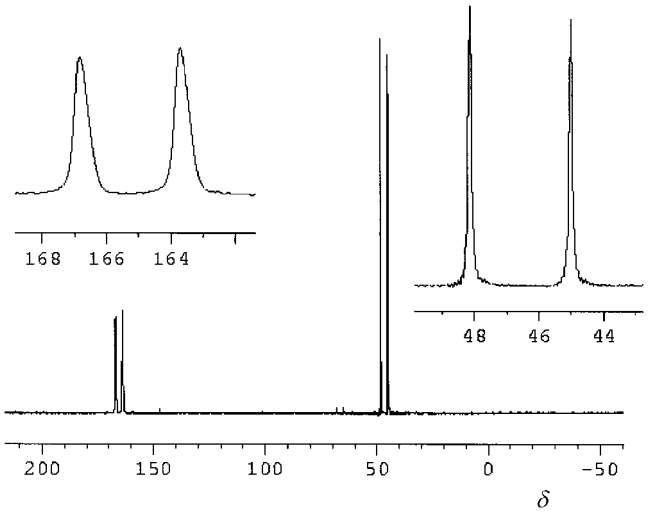

Figure 11. ^{31}P MAS NMR of **3b** at RT with 25 kHz spinning frequency.

This shows that the two phosphorus atoms in $P_2Br_5^+$ appear as doublets at $\delta(^{31}P) = 46.5$ (PBr_3 moiety) and 166.7 (PBr_2 moiety) with $^1J_{PP} = 503$ Hz. In contrast, the low-temperature solution NMR spectrum of **3b** shown in Figure 10 indicated rapid exchange of the dissolved $P_2Br_5^+$ cation.

Comparing the signals in Figure 10 with those of the solid-state NMR spectrum in Figure 11 indicates that the two signals at $\delta(^{31}P) = 155$ and 45 in CD_2Cl_2 at 193 K in Figure 10 are due to rapidly exchanging $P_2Br_5^+$. A possible tentative assignment of the third signal at $\delta(^{31}P) = 228$ could be exchanging PBr_3 (cf. $\delta(^{31}P)$ of free PBr_3 is 228). Upon warming the compound to 193 and 203 K, the signal at $\delta =$ 228 ppm moves to higher field, to 210 ppm. Alternatively, however, the signal at $\delta(^{31}P;\ 193\ K) = 228$ could be due to another isomer of $P_2Br_5^+$, and the similarity of this shift and that of PBr_3 might only be a coincidence. To investigate this possibility, several other $P_2Br_5^+$ isomers were fully optimized at the MP2/TZVPP level, and their relative energies in CH_2Cl_2 were calculated. The MP2 geometries are shown in Figure 12, and the total and relative energies are shown in Table 9.

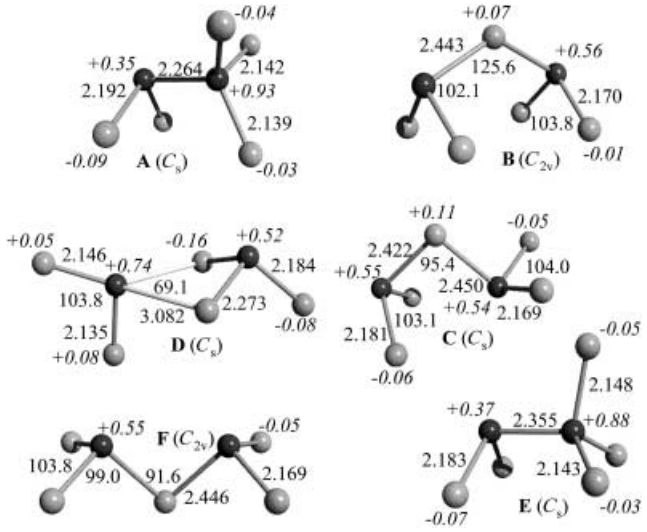

Figure 12. The geometries of six $P_2Br_5^+$ isomers **A**–**F** optimized at the MP2/TZVPP level. Computed partial charges are given in italics.

An analysis of Figure 12 and Table 9 shows that the experimentally found isomer **A** is the global minimum of all the assessed species. Free rotation around the P–P bond to give isomer **E** [$U_{rel.}$(gas, 0 K) = +21.35 kJ mol^{-1}] is very likely in solution; however, it does not explain the third observed NMR shift. The relative energies of the MP2 calculations of all isomers **B**–**D** and **F** are at least 61.96 kJ mol^{-1} higher in energy than isomer **A**. This shows that the signal at $\delta(^{31}P;$ 193 K) = 228 is not due to another isomer of $P_2Br_5^+$ and must be assigned to PBr_3. But where does the free PBr_3 originate from? Hydrolysis was ruled out by preparing several samples

Table 9. Total and relative energies of six $P_2Br_5^+$ isomers **A**–**F** at the MP2/TZVPP level.

	Type					
$P_2Br_5^+$ Isomers	**A** (C_s)	**B** (C_{2v})	**C** (C_s)	**D** (C_s)	**E** (C_s)	**F** (C_{2v})
MP2/TZVPP: U [a.u.]	−13544.51217	−13544.47448	−13544.47902	−13544.45696	−13544.50404	−13544.47650
ZPE (MP2/TZVPP) [a.u.]	0.00830	0.00702	0.00714	Nimag = 1[c]	Nimag = 1[c]	0.00709
H_{solv} (BP86/SVP) COSMO[43] [a.u.]	−0.06013	−0.06177	−0.06131	–	–	−0.06114
PM3: Thermal + Entropic[44] [a.u.]	−0.03859	−0.04133	−0.04580	–	–	−0.04134
$U_{rel.}$(gas, 0 K) [kJ mol^{-1}]	0.00	98.96	87.05	144.96	21.35	93.64
$G_{rel.}$(CH_2Cl_2, 298 K) [kJ mol^{-1}]	0.00	84.07	61.96	–	–	80.58

[a] U_{rel}(gas, 0 K) denotes the relative internal energy at 0 K. [b] $G_{rel.}$(CH_2Cl_2, 298 K) denotes the relative free energy in CH_2Cl_2 solution at 298 K. [c] Transition state with one imaginary frequency.

0947-6539/02/0819-4484 $ 20.00+.50/0 *Chem. Eur. J.* **2002**, *8*, No. 19

of crystalline material of different batches—all samples gave the same spectra as the one shown in Figure 10. Therefore an equilibrium according to Equation (9) might possibly be the reason for the presence of PBr_3 in the solution NMR spectrum of **3b**:

$$P_2Br_5^+ + CH_2Cl_2 \rightleftharpoons PBr_3 + PBr_2^+(CH_2Cl_2) \quad (9)$$

The ^{31}P NMR shift of the naked PBr_2^+ cation would be expected to occur in the range between $\delta = +500$ to $+1000$ ppm and therefore a coordination of at least one molecule of CH_2Cl_2 was also assumed. DFT and MP2 calculations of several isomers of $PBr_2^+(CH_2Cl_2)$ showed that i) coordination of one molecule of CH_2Cl_2 is exothermic (exergonic) by about 75 (50) kJ mol^{-1} and ii) coordination of one molecule of CH_2Cl_2 leads to an upfield shift of several hundred ppm versus the calculated ^{31}P NMR shift of PBr_2^+ of about $+900$ ppm. The exact chemical shift of $PBr_2^+(CH_2Cl_2)$ will be strongly affected by spin–orbit effects,[36] which may lead to a further upfield shift. However, also carefully scanning a chemical shift range of $+1300$ to -1000 ppm at several temperatures between -90 and $-30\,^\circ$C, we never observed another NMR signal that could be assigned to $PBr_2^+(CH_2Cl_2)$. It appears that, due to exchange with PBr_3 and the CH_2Cl_2, the signal due to $PBr_2^+(CH_2Cl_2)$ is invisible in the NMR spectrum. A chemical hint for the possible presence of $PBr_2^+(CH_2Cl_2)$ in solution as an intermediate was given by the following reaction of $[P_2Br_5]^+[Al(OR)_4]^-$ with P_4 kept at $-80\,^\circ$C [Eq. (10):

$$P_2Br_5^+[Al(OR)_4]^- + P_4 \rightarrow P_5Br_2^+[Al(OR)_4]^- + PBr_3 \quad (10)$$

Possibly the proposed $PBr_2^+(CH_2Cl_2)$ intermediate reacted with the P_4 molecule by insertion into the P–P bond to give the $P_5Br_2^+$ cation. The actual spectrum has been deposited. No other ^{31}P NMR signal of an in situ reaction as in Equation (10) kept at $-80\,^\circ$C was observed in the $-90\,^\circ$C ^{31}P NMR spectrum. Therefore, Equation (10) provides evidence for our proposal that dissolved $P_2Br_5^+$ might be in equilibrium with PBr_3 and $PBr_2^+(CH_2Cl_2)$; however, it must be concluded that the solution behavior of the $P_2Br_5^+$ cation is complex and only partly understood. Therefore the equilibrium according to Equation (9) remains only a reasonable working hypothesis.

^{31}P NMR of $P_5X_2^+$: In contrast to **3a** and **b** above, **4a** and **b** are rigid at room temperature and have a first-order spectrum. The structure of the C_{2v}-symmetric P_5 cage of **4a**,**b** followed from the ^{31}P NMR spectrum of the $P_5X_2^+$ cations (X = Br, I; $P_5Br_2^+$ spectrum shown in Figure 13).

As shown in Table 10, the position of the PX_2 moiety in $P_5X_2^+$ is shifted considerably from $\delta(^{31}P) = +23$ (X = Br) to $\delta(^{31}P) = -89$ (X = I) due to an effective Fermi contact mechanism[36] that is also responsible for the extreme upfield shift of the PI_4^+ cation ($\delta(^{31}P;$ **1a**$) = -475$, see above).

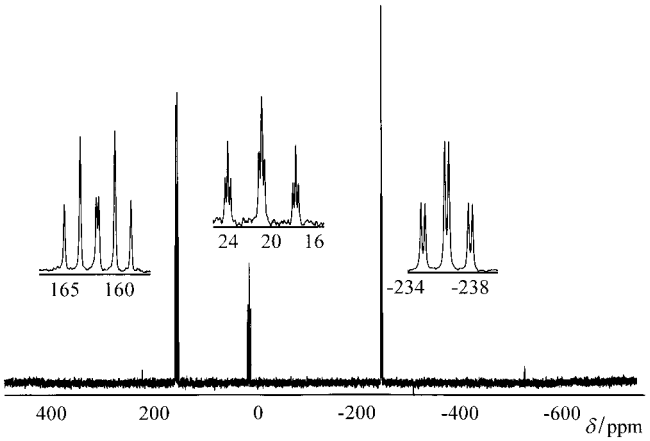

Figure 13. ^{31}P NMR spectrum of **4b** in CD_2Cl_2 at $-70\,^\circ$C.

Table 10. Summary of the ^{31}P NMR shifts of the known binary P–X cations. P_A, P_B, and P_C denote the following nuclei: $P_AX_4^+$, X_2P_A-$P_BX_3^+$, and $X_2P_A(P_B)_2(P_C)_2^+$.

Compound	$\delta(^{31}P_A)$	$\delta(^{31}P_B)$	$\delta(^{31}P_C)$
$PI_4^+[Al(OR)_4]^-$ **1a**	-475 (223 K)	–	–
$PI_4^+SbF_6^-$[36]	-519[a]	–	–
$PBr_4^+[Al(OR)_4]^-$ **1b**	-83 (283 K)	–	–
$PBr_4^+AsF_6^-$[1b]	-83[a]	–	–
$P_2I_5^+[Al(OR)_4]^-$ **3a**	$+126$ (183 K)	-156 (183 K)	–
$P_2I_5^+AlI_4^-$[3a]	$+114$[a]	-142[a]	–
$P_2Br_5^+[Al(OR)_4]^-$ **3b**	$+165.7$ ($^1J_{PP} = 503$ Hz)[a]	$+46.5$ ($^1J_{PP} = 503$ Hz)[a]	–
$P_2Br_5^+[Al(OR)_4]^-$ **3b**	$+155$ (183 K, br)	$+45$ (183 K, br)	–
$P_5I_2^+[Al(OR)_4]^-$ **4a**	-89 (193 K)	$+168$ (193 K)	-194 (193 K)
$P_5Br_2^+[Al(OR)_4]^-$ **4b**	$+23$ (193 K)	$+163$ (193 K)	-236 (193 K)

[a] Solid-state MAS NMR at RT.

Thermodynamics of the formation of PX_2^+, PX_4^+, $P_2I_3^+$, P_2X_5, and $P_5X_2^+$: The thermochemistry of the formation of the P–X cations was assessed in the gas phase and in CH_2Cl_2 with the COSMO model by including approximate free solvation energies.[43] All values given include the ZPE and thermal corrections to the enthalpy (H) or the free energy (G)[44] at a temperature of 298 K [Eqs. (a)–(h) in Table 11]. To establish the quality of the calculations, we independently calculated Δ_rH^{298} for the reaction of gaseous $P_3^+ + Br_2 \rightarrow PBr_2^+ + 0.5\,P_4$ [(Eq. (11)] based on the published enthalpies of formation at 298 K[7, 45, 53]

$$P_3^+ + Br_2 \rightarrow PBr_2^+ + 0.5\,P_4 \quad (11)$$
$$\Delta_rH^{298} = -148 \text{ kJ mol}^{-1}\text{[45]} \text{ (enthalpies of formation)}$$
$$\Delta_rH^{298} = -142 \text{ kJ mol}^{-1} \text{ (MP2/TZVPP)}$$

Our MP2 value of -142 kJ mol^{-1} and the enthalpy from Equation 10 (derived from the experimentally determined heats of formation) of -148 kJ mol^{-1}[45] agree very nicely within 6 kJ mol^{-1}. Therefore it is reasonable to suggest that that the enthalpies of reactions collected in Table 11 below will be accurate to a similar order of magnitude. The thermochemistry of the formation of all the cations prepared here is presented in Table 11, below.

  0947-6539/02/0819-4485 $ 20.00+.50/0

Table 11. MP2/TZVPP calculated enthalpies and free energies[44] of reaction at 298 K [kJ mol^{-1}] for the formation of the P–X cations (X = Br, I) in the gas phase and in CH_2Cl_2 (COSMO model).[43] The values in parenthesis include the formation of solid AgX.

Reaction	X = I: $\Delta_r H_{(gas)}$	X = Br: $\Delta_r H_{(gas)}$	X = I: $\Delta_r G_{(CH_2Cl_2)}$	X = Br: $\Delta_r G_{(CH_2Cl_2)}$
(a) $Ag^+ + PX_3 \rightarrow PX_2^+ + AgX$	+43.9 (−153.0)[a]	+91.9 (−125.5)[b]	+63.6 (−100.3)[c]	+81.5 (−101.8)[d]
(b) $Ag^+ + X_2 + PX_3 \rightarrow PX_4^+ + AgX$	−177.6 (−374.5)[a]	−183.0 (−400.4)[b]	−69.8 (−233.7)[c]	−102.4 (−284.7)[d]
(c) $PX_2^+ + X_2 \rightarrow PX_4^+$	−217.1	−274.9	−133.5	−183.9
(d) $Ag^+ + 2\,PX_3 \rightarrow P_2X_5^+ + AgX$	−177.7 (−374.6)[a]	−99.7 (−317.1)[b]	−42.8 (−206.7)[c]	+0.3 (−182.0)[d]
(e) $PX_2^+ + PX_3 \rightarrow P_2X_5^+$	−221.6	−191.6	−106.5	−81.2
(f) $Ag^+ + P_4 + PX_3 \rightarrow P_5X_2^+ + AgX$	−145.5 (−342.1)[a]	−112.3 (−329.7)[b]	−49.6 (−213.5)[c]	−32.7 (−215.0)[d]
(g) $PX_2^+ + P_4 \rightarrow P_5X_2^+$	−188.6	−210.6	−113.2	−114.2
(h) $Ag^+ + P_2I_4 \rightarrow P_2I_3^+ + AgX$	+14.6 (−182.3)[a]	–	−6.7 (−170.3)[c]	–

[a] The enthalpy for the process $AgI_{(g)} \rightarrow AgI_{(s)}$ is −196.9 kJ mol^{-1}. [b] The enthalpy for the process $AgBr_{(g)} \rightarrow AgBr_{(s)}$ is −217.4 kJ mol^{-1}. [c] The enthalpy for the process $AgI_{(solv)} \rightarrow AgI_{(s)}$ in CH_2Cl_2 is −163.6 kJ mol^{-1}. [d] The enthalpy for the process $AgBr_{(solv)} \rightarrow AgBr_{(s)}$ in CH_2Cl_2 is −182.3 kJ mol^{-1}.

From Equation (a), the intermediate presence of PX_2^+ follows when the formation of solid AgX is assumed. However, this cation rapidly reacts with X_2, PX_3, or P_4 according to Equations (c), (e), or (g) to give PX_4^+, $P_2X_5^+$, and $P_5X_2^+$ so that the overall reactions as in Equations (b), (d), or (f) are highly favored. The intermediate formation of $P_2I_3^+$ from P_2I_4 and Ag^+ proposed above appears very likely since reaction (h) in Table 11 is exergonic in solution even without formation of solid AgI, which further favors the formation of $P_2I_3^+$.

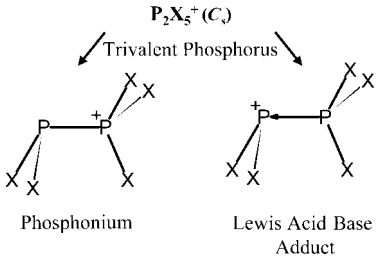

Scheme 2. Possible bonding descriptions of the $P_2X_5^+$ cation: phosphonium cation or Lewis acid base adduct.

Structure and bonding of the P–X cations:

The PX_4^+ cations: As seen by the good agreement between experimental and MP2-optimized geometries, the PX_4^+ cations in **1a**,**b** represent naked isolated cations similar to the gas phase situation (see Table 12). The phosphonium character of the P atom in PX_4^+ is evident from the calculated partial charges, which grew from $\Delta q = +0.38$ to $+0.59$ on going from $P^{III}X_3$ to $P^{V}X_4^+$ (Table 12). Compared with PX_3, the P–X bonds are shortened by 0.06 to 0.11 Å. This is also reflected in the increase in the calculated *SEN*s of the P–X bonds, which grew from 1.03 – 1.06 in PX_3 to 1.09 – 1.12 in the PX_4^+ cations. Both are attributed to the higher charge of and therefore the contracted orbitals of the P^V center in PX_4^+, which also lead to higher coulombic contributions to the bonding here than in $P^{III}X_3$ (cf. P and X partial charges).

Pentavalent neutral P^VI_5 is unknown[6, 46]—however, it may be $I_2 \leftarrow PI_3$—and it was argued that the positive charge stabilizes the PI_4^+ cation against the loss of I_2 and formation of the unstable PI_2^+.

The $P_2X_5^+$ cations: Two competing simple bonding descriptions of the $P_2X_5^+$ cation are possible and shown in Scheme 2: either a) the tetracoordinate phosphorus atom is a phosphonium center, and therefore the P–P bond lengths fall into the normal range of a P–P single bond (about 2.21 Å) or b) the $P_2X_5^+$ cation may be described as a Lewis acid base adduct of the PX_2^+ cation acting as a Lewis acid toward the PX_3 Lewis base. Therefore a longer dative P–P bond is expected as, for example, in the $Mes^*NP^+ \leftarrow PPh_3$ cation, in which the Mes^*NP^+ acid is stabilized by a PPh_3 base; this leads to a long dative P–P bond length of 2.625(2) Å ($Mes^* = 2,4,6\text{-}t\text{Bu}_3C_6H_2$).[47]

In the solid state, the normal to slightly elongated P–P bond lengths of 2.22(1) to 2.246(3) Å in **3a**,**b**, **5**, and $P_2I_5[AlI_4]$[2] clearly show that the phosphonium description as in Scheme 2 is correct (see structural data in Table 13). However, DFT and HF-DFT calculations considerably overestimate the lengths of the P–P bond by 0.1 to 0.2 Å regardless of the type and size of the basis sets employed,[4] that is also with flexible all-electron basis sets or quasi-relativistic ECP cores and a flexible description of the valence electrons. DFT and HF-DFT calculations appear to favor the Lewis acid base description, as in Scheme 2, while MP2 gives a phosphonium species that was also observed in the solid state. The ambiguity of the bonding of the $P_2X_5^+$ cations is also reflected in their unusual solution behavior. $P_2I_5^+$ slowly disproportionates into the reduced $P_3I_6^+$ and the oxidized PI_4^+, while

Table 12. Experimental and MP2/TZVPP-calculated structural parameters of the PX_4^+ cations (X = Br, I) in PI_4AlCl_4, PBr_4Br, and **1a**,**b**.

Parameter	**1a**	PI_4AlCl_4	MP2	**1b**	PBr_4Br	MP2
$P–X_{av.}$ [Å]	2.3700(4)	2.368(4)	2.373	2.1106(9)	2.15(3)	2.130
$P–X_{range}$ [Å]	–	2.361(4)-2.372(4)	–	–	2.13(3) – 2.17(3)	–
$X\text{-}P–X_{range}$ [°]	109.1(1) – 109.6(1)	108.4(2) – 110.1(2)	109.5	109.2(1) – 109.9(1)	107.9(16) – 110.0(10)	109.5
q(P)	–	–	+0.48[a]	–	–	+1.10[b]
q(X)	–	–	+0.13[a]	–	–	−0.03[b]
SEN(P–X)	–	–	1.09[a]	–	–	1.12[b]

[a] PI_3 values for comparison: $q(P) = 0.11$, $q(I) = -0.04$, $SEN(P–I) = 1.06$. [b] PBr_3 values for comparison: $q(P) = 0.51$, $q(Br) = -0.17$, $SEN(P–Br) = 1.03$.

0947-6539/02/0819-4486 $ 20.00+.50/0 *Chem. Eur. J.* **2002**, *8*, No. 19

Table 13. Experimental and MP2/TZVPP-calculated structural parameters[a] of the $P_2X_5^+$ cation (X = Br, I) in $P_2I_5AlI_4$, **3a**,**b** and **5**.

Parameter	**3a** (200 K)	**5**	$P_2I_5AlI_4$	MP2	**3b** (200 K)	**3b** (150 K)	MP2
P1-P2	2.24(1)	2.240(7)	2.22(1)	2.253	2.248(7)	2.246(3)	2.264
P1-X1	2.378(7)	2.394(4)	2.399(9)	2.375	2.169(6)	2.129(2)	2.139
P1-X2	2.361(7)	2.390(4)	2.399(9)	2.376	2.139(6)	2.115(2)	2.142
P1-X3	2.367(8)	2.369(4)	2.409(10)	2.376	2.156(6)	2.129(2)	2.142
P1-$X_{1,2,3}$ (av.)	2.369	2.384	2.403	2.376	2.154	2.124	2.141
P2-X4	2.48(1)	2.460(5)	2.420(9)	2.413	2.158(6)	2.199(3)	2.192
P2-X5	2.43(1)	2.451(4)	2.419(9)	2.413	2.221(6)	2.184(3)	2.192
P2-$X_{4,5}$ (av.)	2.455	2.455	2.420	2.413	2.190	2.192	2.192
P2-P1-X1	114.2(4)	116.3(2)	–	110.6	106.9(3)	115.5(1)	115.1
P2-P1-X2	109.1(4)	106.4(2)	–	105.0	107.6(3)	106.1(1)	106.8
P2-P1-X3	104.7(4)	103.8(2)	–	105.0	104.6(3)	106.4(1)	106.8
P1-P2-X4	92.3(4)	95.3(3)	–	97.0	93.2(2)	95.1(1)	95.1
P1-P2-X5	92.6(4)	94.6(3)	–	97.0	91.4(2)	93.7(1)	95.1
X1-P1-X2	104.5(3)	110.7(2)	108.4(4)	110.2	109.4(2)	108.8(1)	109.5
X2-P1-X3	113.9(3)	108.4(2)	108.8(4)	109.0	117.0(2)	110.5(1)	109.1
X3-P1-X1	110.7(3)	110.9(2)	109.3(4)	110.2	110.9(2)	109.5(1)	109.5
X4-P2-X5	102.2(4)	104.1(3)	103.8(4)	105.3	112.8(2)	104.2(1)	104.5

[a] Labeling as in 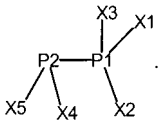

.

$P_2Br_5^+$, with a slightly longer and thus weaker P–P bond[48] than $P_2I_5^+$ (Table 13), appears to be in equilibrium with $PBr_2^+(CH_2Cl_2)$ and PBr_3. Both observations and calculations indicate that the P–P bond resides in a shallow potential where larger deviations from the equilibrium geometry only lead to small increases of the overall energy. This may be attributed to the partially π-bonded nature of the free PX_2^+ cation, in which the formation of one additional π bond compensates for the loss of a P–P σ bond (Figure 14) and therefore accounts for the difficulties in computationally modeling the $P_2X_5^+$ cations as well as the observed dissociation reactions of the $P_2X_5^+$ cations in **3a**,**b**.

The $P_5X_2^+$ cations: The P_5 cage of **4a**,**b** is without precedence,[20] and the range of the P–P bond lengths in the $P_5Br_2^+$ cation of 2.150(7) to 2.262(8) Å resembles values found for P–P single bonds as in P_4 (2.21 Å) or $Ag(P_4)_2^+$ (2.15 to 2.32 Å).[10, 11] The P–Br distances of 2.140(3) Å are short relative to *d*(P–Br) = 2.22 Å in PBr_3. Ab initio MP2/TZVPP and HF-DFT MPW1PW91/6-311GG(2df)[49, 50] calculations reproduced the solid-state geometry of $P_5Br_2^+$ to within 0.024 Å and 1.2°. $P_5Br_2^+$ is a true minimum at both levels; calculated and experimental structural parameters are compared in Table 14. For comparison the MP2/TZVPP-calculated $P_5I_2^+$ geometry is also included.

The calculated Roby–Davidson (NBO[14]) partial charges at the MP2 (HF-DFT) level suggest that part of the unipositive charge of the $P_5Br_2^+$ cation is delocalized over the P_5 cage with a high +0.89 (+0.47) partial charge residing on the phosphonium atom P1 and lower charges of +0.05 (+0.15) on P2,3 or +0.10 (+0.13) on P4,5. The more electronegative Br1,2 atoms are slightly negative (−0.09 or −0.02). The shorter P–P bond lengths of 2.156(7) Å around the tetracoordinate P1 atom are not reflected in an increase in the *SEN* of the P–P bond and all *SEN*(P–P) in $P_5Br_2^+$ ($P_5I_2^+$) range from 1.21 to 1.27 (1.20 to 1.26) (cf. *SEN*(P_4) = 1.26). Therefore it is likely that the shortening of the P_1–$P_{2,3}$ bond lengths by about 0.05 to 0.07 Å is due to the onium character of P1, with contracted orbitals and a smaller covalent radius leading to the shorter P–P bonds but no increase in the bond order or the *SEN*.

PX_2^+—An intermediate on the pathway to PX_4^+, $P_2X_5^+$, and $P_5X_2^+$? We have shown above that the intermediate formation of PX_2^+ cations is thermodynamically possible if the (observed) formation of solid AgX is assumed (Table 11). Intermediate PX_2^+ formation is also in agreement with the observation that AgX is immediately formed when solid or liquid PX_3 is added to solutions of $AgAl(OR)_4$ in CH_2Cl_2 at

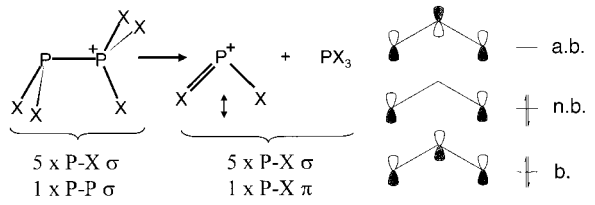

Figure 14. Compensation for the P–P σ bond in $P_2X_5^+$ by an P–X π bond in PX_2^+ upon dissociation; bonding (b), nonbonding (nb), and antibonding (ab) π MOs of PX_2^+.

Table 14. Structural parameters of the $P_5X_2^+$ cations averaged according to local C_{2v} symmetry (X = Br, I); separations in Å and angles in °.

Param.	$P_5Br_2^+$ Exp.	$P_5Br_2^+$ MP2[a]	$P_5Br_2^+$ MPW1PW91[b]	$P_5I_2^+$ MP2[a]
P–X	Br: 2.140(3)	Br: 2.163	Br: 2.164	I: 2.383
P_1-$P_{2,3}$	2.156(7)	2.167	2.171	2.181
$P_{2,3}$-$P_{4,5}$	2.239(8)	2.259	2.239	2.254
P_4-P_5	2.211(8)	2.222	2.194	2.229
X-P-X	Br: 106.4(2)	Br: 105.8	Br: 106.1	I: 108.5
$P_{2,3}$-P_1-X	Br: 114.7(3)	Br: 114.6	Br: 115.0	I: 114.2
P_2-P_1-P_3	91.4(3)	92.6	90.9	90.9
$P_{4,5}$-$P_{2,3}$-P_1	83.0(3)	82.0	83.1	83.1
$q(P_1)$	–	+0.89	+0.47[c]	+0.57
$q(P_{2,3})$	–	+0.05	+0.15[c]	+0.05
$q(P_{4,5})$	–	+0.10	+0.13[c]	+0.09
q(X)	–	−0.09	−0.02[c]	+0.07

[a] TZVPP basis set. [b] 6–311G(2df) basis set. [c] NBO charges at the MPW1PW91/6–311G(2df) level.[14]

$-78\,^{\circ}C$. The following reactions of the PX_2^+ cation intermediates with X_2, PX_3, and P_4 are highly exothermic and favored by -191.6 to $-274.9\,kJ\,mol^{-1}$ ($\Delta_r H$ in the gas phase, see Table 11). We understand the formations PX_4^+, $P_2X_5^+$, and $P_5X_2^+$ as well as $P_3I_6^+$[4] to be insertion reactions of the electrophilic carbene-analogous PX_2^+ intermediate into the bonds of X_2, PX_3, P_4, and P_2I_4 as shown in Scheme 3.

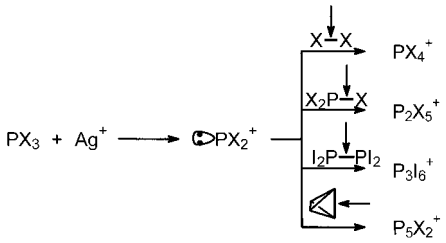

Scheme 3. PX_2^+ insertion reactions. Bonds where PX_2^+ is assumed to insert are labeled with an arrow.

The intermediate presence of PX_2^+ cations was further supported by the solution behavior of $P_2Br_5^+$; here the $P_2Br_5^+$ cation in **3b** served as a PBr_2^+ source when treated with P_4 at $-80\,^{\circ}C$ and gave $P_5Br_2^+$ and PBr_3 (^{31}P NMR at $-90\,^{\circ}C$, see above). The carbene-like behavior of PR_2^+ cations (R = H, Cl, NH_2, OH, SH, organo) was earlier investigated on theoretical grounds.[51] In agreement with our results, it followed from this paper that only for electronegative ligands R with little π back donation—that is, R = H, Cl—should the PR_2^+ cation act as an electrophilic carbene analogue with a HOMO mainly residing on the phosphorus atom. With stronger π back donation, as for R = OH, NH_2, the HOMO is centered on the oxygen or nitrogen atoms.[51] We consistently calculated lower *SEN*s of 1.35 to 1.38 for the P–X bonds in PX_2^+ (expected: 1.50) and higher positive partial charges of $+0.39$ to $+0.73$ to reside on the P atoms; a visualization of the MOs of PX_2^+ at the MP2 level verified that the HOMO is P-centered.

Stability of the $Al(OR)_4^-$ anion in comparison with EF_6^- (E = As, Sb): Previous attempts to prepare $P_2I_5^+$ salts by reaction of $I_3^+MF_6^-$ (M = As, Sb) with P_2I_4 in various solvents failed, leading to immediate decomposition and formation of PF_3, I_2, and MI_3 even at $-78\,^{\circ}C$.[3] The more stable $PI_4^+MF_6^-$ salts were also shown to decompose in the solid state at around $0\,^{\circ}C$.[6] To put this qualitative picture on a quantitative basis, we assessed the decomposition of the hypothetical $[P_2I_5]^+[AsF_6]^-$ based on the published enthalpies of formation of gaseous AsF_6^- ($-1919\,kJ\,mol^{-1}$),[40a] gaseous PF_3 ($-958.4\,kJ\,mol^{-1}$),[7] solid AsI_3 ($-58.2\,kJ\,mol^{-1}$),[7] and solid I_2 ($0\,kJ\,mol^{-1}$)[7] as well as our enthalpy of formation of gaseous $P_2I_5^+$ ($749\,kJ\,mol^{-1}$) assessed above and the estimated lattice potential enthalpy $\Delta H_{Latt.}$ of a hypothetical $[P_2I_5]^+[AsF_6]^-$ salt ($427\,kJ\,mol^{-1}$)[52] as in Scheme 4.

From Scheme 4 it follows, in agreement with experiment,[3] that a hypothetical solid $[P_2I_5]^+[AsF_6]^-$ salt is unstable toward decomposition into $2\,PF_{3(g)}$, solid AsI_3 and I_2 by $379\,kJ\,mol^{-1}$. This instability may be contrasted with the fact that solid samples of **1a**,**b** and **3a**,**b** are stable at room temperature for days. The isolation of **1a**,**b**, **3a**,**b**, and **4a**,**b** is therefore only consequent, and due to the higher (kinetic) stability of the $Al(OR)_4^-$ anion relative to the MF_6^- class of ions.

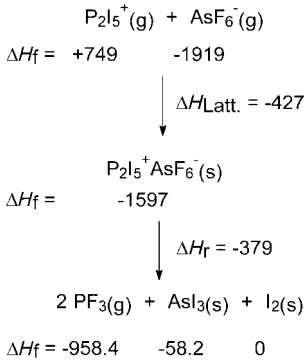

Scheme 4. Scheme used to estimate the enthalpy of reaction for the decomposition of solid $P_2I_5^+AsF_6^-$ into $2\,PF_{3(g)}$, solid AsI_3 and I_2. All values given are in $kJ\,mol^{-1}$, and the enthalpies of formation ΔH_f at 298 K are written below the respective species.

Conclusion

Silver-salt metathesis of $Ag[Al(OR)_4]$ with PX_3 generated the highly reactive PX_2^+ intermediates. For $R = CH(CF_3)_2$, all generated cations fully decomposed the anion, but with $R = C(CF_3)_3$ moderately stable P–X cation salts were obtained. The PX_2^+ intermediates acted as an electrophilic carbene analogue[51] and inserted themselves into the X–X, P–X, or P–P bond of X_2, PX_3, or P_4 to quantitatively give stable but highly electrophilic and soluble PX_4^+, $P_2X_5^+$, and phosphorus-rich $P_5X_2^+$,[14] as well as subvalent $P_3I_6^+$[4] salts of the weakly basic $Al[OC(CF_3)_3]_4^-$ anion. Previously PX_2^+ cations (X = Cl, Br, I) were only investigated in the gas phase.[51, 53, 54] Dissolved $P_2X_5^+$ is fluxional on the timescale of ^{31}P NMR spectroscopy and disproportionates for X = I in a time- and concentration-dependent manner into the reduced $P_3I_6^+$ and an oxidized species that was assigned as PI_4^+. $P_2Br_5^+$ is even more fluxional than $P_2I_5^+$ and may be in equilibrium with $PBr_2^+{}_{(CH_2Cl_2)}$ and PBr_3. The loss of one P–P σ bond energy upon dissociation of $P_2Br_5^+$ is partially compensated for by P–Br π-bond formation in PBr_2^+, which may facilitate the dissociation. The phosphorus-rich $P_5X_2^+$ cations are the first binary P–X cations that include a phosphorus cage and are the closest approximation of the homopolyatomic phosphorus cations, which are as yet unknown on a preparative scale.[4] Further efforts will be directed toward the synthesis of new examples of P-rich binary P–X or pure P cations.

Silver-salt metathesis reactions of the very reactive $Ag[Al(OR)_4]$ salt with elemental halides provide an alternative approach to polyatomic nonmetal cations that are conventionally prepared by direct oxidation with strong one- or two-electron oxidizers such as PtF_6, WX_6 (X = F, Cl), MF_5 (M = As, Sb,[40a] Nb, Au[55]) or strong Lewis acids such as AlX_3 (X = Cl, Br, I)[40a] and transition metal halides or oxohalides.[56] The silver-salt metathesis approach allows reduced subvalent cations that are difficult to prepare by oxidative approaches to be stabilized. Moreover, the $Al(OR)_4^-$ salts are highly soluble in moderately polar solvents such as CH_2Cl_2 even at low temperatures and therefore allow the often fluxional

0947-6539/02/0819-4488 $ 20.00+.50/0 *Chem. Eur. J.* **2002**, *8*, No. 19

cations to be studied in detail by low-temperature NMR spectroscopy.

Experimental Section

All manipulations were performed by using grease-free Schlenk or dry-box techniques and a dinitrogen or argon atmosphere. All apparatus were closed by J. Young valves. The solvents were rigorously dried over P_2O_5, stored under N_2 on molecular sieves (4 Å), and degassed prior to use. PI_3 and P_2I_4 were prepared from stoichiometric amounts of (sublimed) P_4 and iodine in CS_2 solution and their purity was checked by Raman spectroscopy. PBr_3 was purchased from Merck and distilled prior to use. Yellow P_4 was melted, filtered through a fine sintered-glass frit and sublimed prior to use. The silver aluminates $Ag[Al(OR)_4]$ were prepared according to the literature.[9] Raman and IR spectra were recorded with a 1064 nm laser on a Bruker IFS66v spectrometer equipped with the Raman module FRA106. IR spectra were recorded in Nujol mull between CsI plates, and Raman spectra were obtained from solid samples sealed in a melting point capillary or (better) a 5 mm NMR tube. NMR spectra of sealed samples were run on a Bruker AC250 spectrometer and were referenced to the solvent (^{13}C) or external C_6F_6 (^{19}F), H_3PO_4 (^{31}P), or aqueous $AlCl_3$ (^{27}Al). The ^{31}P MAS NMR spectrum was obtained on a Bruker DSX400 spectrometer with a frequency of 161.97 MHz and a spinning frequency of 25000 Hz, d1 (trigger time) 360 s; standard: 1M H_3PO_4. Data of the vibrational spectra were included into the text (cations) or were deposited (anion bands).

Synthesis of $[PI_4]^+[Al(OR)_4]^-$ (1a): $Ag(CH_2Cl_2)[Al(OR)_4]$ (0.747 g, 0.64 mmol), I_2 (0.163 g, 0.64 mmol), and PI_3 (0.265 g, 0.64 mmol) were weighed into one bulb of a single-piece apparatus.[58] CH_2Cl_2 (ca. 20 mL) was condensed onto the solid mixture at 77 K, and the resulting suspension was stirred overnight at −30 °C. The resulting orange solution was filtered, concentrated to about 5 mL, and cooled to −30 °C overnight. Large orange blocks of $PI_4^+[Al(OR)_4]^-$ (**1a**) crystallized and were isolated (0.83 g, 86 %). ^{13}C NMR (63 MHz, CD_2Cl_2, 25 °C): $\delta = 121.7$ (q, CF_3, $J_{CF} = 293.3$ Hz); ^{27}Al NMR (78 MHz, CD_2Cl_2, 25 °C): $\delta = 38.8$ (s, $\tilde{\nu}_{1/2} = 9$ Hz); ^{31}P NMR (101 MHz, CD_2Cl_2, −50 °C): $\delta = -475$ ($\tilde{\nu}_{1/2} = 330$ Hz).

In situ NMR reaction according to Equation (1): $Ag(CH_2Cl_2)[Al(OR)_4]$ (0.108 g, 0.093 mmol), I_2 (0.028 g, 0.110 mmol), and PI_3 (0.039 g, 0.095 mmol) were weighed into a NMR tube glass-blown onto a valve. CD_2Cl_2 (0.7 mL) was condensed onto the mixture at 77 K, and the sealed tube was then stored at −30 °C and occasionally heavily shaken. Solid yellow AgI formed in an orange-brown solution. ^{31}P NMR spectra of this sample were recorded after 12 h and showed the (broad) signal of PI_4^+, shown in the upper trace of a deposited figure ($\delta(^{31}P; -50\,^\circ C) = -475$ (s, 1P, $\tilde{\nu}_{1/2} = 1370$ Hz)).

Synthesis of $[PBr_4]^+[Al(OR)_4]^-$ (1b): $Ag(CH_2Cl_2)[Al(OR)_4]$ (0.661 g, 0.57 mmol), Br_2 (0.03 mL, 0.57 mmol), and PBr_3 (0.054 mL, 0.57 mmol) were put into one bulb of a single-piece apparatus.[58] CH_2Cl_2 (ca. 7 mL) was added to the mixture at −78 °C, and the mixture was stirred overnight at −30 °C. The resulting slightly yellowish solution over colorless precipitate (0.106 g, calcd AgBr: 0.107 g) was filtered, concentrated to about 5 mL, and cooled to −30 °C overnight. Long colorless needles of $PBr_4^+[Al(OR)_4]^-$ (**1b**) crystallized and were isolated (0.198 g, 26 %). The yield was improved by further concentration of the filtrate and cooling to −30 °C to give another 0.324 g of **1b**, a total yield of 69 %. ^{13}C NMR (63 MHz, CD_2Cl_2, +10 °C): $\delta = 121.5$ (q, $J_{CF} = 293.4$ Hz, CF_3); ^{19}F NMR (376 MHz, CD_2Cl_2, +10 °C): $\delta = -73.7$; ^{27}Al NMR (78 MHz, CD_2Cl_2, +10 °C): $\delta = 36.2$ (s, $\tilde{\nu}_{1/2} = 11$ Hz); ^{31}P NMR (101 MHz, CD_2Cl_2, +10 °C): $\delta = -83$.

Attempted in situ preparation of $[P_2I_7]^+[Al(OR)_4]^-$: $Ag(CH_2Cl_2)$-$[Al(OR)_4]$ (0.182 g, 0.157 mmol), I_2 (0.040 g, 0.157 mmol), and PI_3 (0.130 g, 0.314 mmol) were weighed into a NMR tube glass-blown onto a valve. CD_2Cl_2 (0.7 mL) was condensed onto the mixture at 77 K, and the sealed tube was then stored at −30 °C and occasionally heavily shaken. Solid yellow AgI formed in an intensely brown-red solution. ^{31}P NMR spectra of this sample were recorded after 12 h and showed the very broad signal of PI_4^+ ($\delta(^{31}P; -90\,^\circ C) = -475$). In a preparative reaction—$Ag(CH_2Cl_2)[Al$-$(OR)_4]$ (0.243 g, 0.210 mmol), I_2 (0.053 g, 0.210 mmol), and PI_3 (0.172 g, 0.420 mmol) in CH_2Cl_2 (10 mL)—large amounts of $PI_4^+[Al(OR)_4]^-$ (**1a**) crystallized from the filtered and concentrated solution (unit cell determination, NMR) while unreacted PI_3 remained with the insoluble compounds (Raman).

Synthesis of $[P_2I_5]^+[Al(OR)_4]^-$ (3a): $Ag(CH_2Cl_2)[Al(OR)_4]$ (1.966 g, 1.695 mmol) and PI_3 (1.396 g, 3.391 mmol) were weighed into one bulb of a single-piece apparatus.[58] CH_2Cl_2 (ca. 35 mL) was condensed onto the solid mixture at 77 K, and the resulting suspension was stirred at −30 °C until all visible PI_3 was consumed (1–2 h). The resulting yellow solution over AgI was filtered, and all volatile compounds were removed in vaccuo to leave $P_2I_5^+[Al(OR)_4]^-$ (**3a**) as a yellow powder (AgI + **3a** calcd: 3.218 g, found: 3.180 g). Isolated yield of **3a**: 2.383 g (85 %); ^{13}C NMR (63 MHz, CD_2Cl_2, 25 °C): $\delta = 122.0$ (q, $J_{CF} = 292.9$ Hz, CF_3); ^{27}Al NMR (78 MHz, CD_2Cl_2, 25 °C): $\delta = 36.0$ (s, $\tilde{\nu}_{1/2} = 9$ Hz); ^{31}P NMR (101 MHz, CD_2Cl_2, 25 °C): $\delta = 35$ ($\tilde{\nu}_{1/2} = 1580$ Hz); $\delta(^{31}P; 101$ MHz, CD_2Cl_2, −90 °C) = 124.9 (s, 1P, $\tilde{\nu}_{1/2} = 290$ Hz), −154.5 (s, 1P, $\tilde{\nu}_{1/2} = 580$ Hz); $AlC_{16}F_{36}I_5O_4P_2$ (M_r = 1663.60): I calcd 38.1 %, found 38.4 %. Compound **3a** is highly soluble[57] and stable in cold CH_2Cl_2 and 1,2-$Cl_2C_2H_4$ ($T \le -20\,^\circ C$). It is also soluble in $CHCl_3$, but slowly decomposes with formation of P_2I_4 (Raman, unit cell determination) and other as yet unidentified products. Attempts to dissolve **3a** in dry $HOC(H)(CF_3)_2$ or CH_3CN also led to decomposition and precipitation of an orange material that contained P_2I_4 (Raman) in a clear colorless solution that did not contain phosphorus species (NMR). It appeared that $C_6H_5CF_3$ and 1,3-$(CF_3)_2C_6H_4$ were also attacked by **3a** (dark coloring of the solution). Solutions of **3a** in CH_2Cl_2 may be handled briefly at room temperature. Solid yellow **3a** is stable for at least 3 months at RT and longer if stored at −30 °C (IR).

Synthesis of $[P_2Br_5]^+[Al(OR)_4]^-$ (3b): $Ag(CH_2Cl_2)[Al(OR)_4]$ (0.803 g, 0.69 mmol) and PBr_3 (0.132 mL, 1.38 mmol) were put into one bulb of a single-piece apparatus.[58] CH_2Cl_2 (ca. 7 mL) was added to the mixture at −78 °C, and the mixture was kept for two days at −30 °C. The resulting slightly yellowish suspension was filtered (0.098 g residue, calcd AgBr: 0.129 g), concentrated to about 3 mL, and cooled to −78 °C overnight. Large yellowish blocks of $P_2Br_5^+[Al(OR)_4]^-$ (**3b**) crystallized and were isolated (0.661 g; 67 %). ^{13}C NMR (63 MHz, CD_2Cl_2, −30 °C): $\delta = 121.2$ (q, $J_{CF} = 293.1$ Hz, CF_3); ^{19}F NMR (376 MHz, CD_2Cl_2, −30 °C): $\delta = -73.7$; ^{27}Al NMR (78 MHz, CD_2Cl_2, −30 °C): $\delta = 37.5$ (s, $\tilde{\nu}_{1/2} = 13$ Hz); ^{31}P NMR (101 MHz, CD_2Cl_2, −90 °C): $\delta = -228$ (br), −155 and 45 (br); ^{31}P NMR (101 MHz, CD_2Cl_2, −50 °C): $\delta = -150$. The −90 °C ^{31}P NMR spectrum of **3b** is shown in Figure 10.

In situ NMR synthesis of $[P_5I_2]^+[Al(OR)_4]^-$ (4a): $Ag(CH_2Cl_2)[Al(OR)_4]$ (0.262 g, 0.22 mmol), P_4 (0.028 g, 0.22 mmol), and PI_3 (0.091 g, 0.22 mmol) were weighed into a NMR tube glass-blown onto a valve. CD_2Cl_2 (0.7 mL) was condensed onto the mixture at 77 K, and the sealed tube was then stored at −80 °C and occasionally heavily shaken. Solid yellow AgI formed in a yellow colored solution. NMR spectra of this sample were recorded after 12 h and showed the exclusive presence of the $[P_5I_2]^+[Al(OR)_4]^-$ salt: ^{19}F NMR (376 MHz, CD_2Cl_2, −70 °C): $\delta = -73.6$ (s); ^{27}Al NMR (78 MHz, CD_2Cl_2, −30 °C): $\delta = 37.5$ (s, $\tilde{\nu}_{1/2} = 15$ Hz); ^{31}P NMR (101 MHz, CD_2Cl_2, −80 °C): $\delta = 168.2$ (dt, $^1J_{P2,3\text{-}P1} = 278.5$ Hz, $^1J_{P2,3\text{-}P4,5} = 152.6$ Hz, 2P), −89.0 (tt, $^1J_{P1\text{-}P2,3} = 278.5$ Hz, $^2J_{P1\text{-}P4,5} = 26.7$ Hz, 1P), −193.9 (td, $^1J_{P4,5\text{-}P2,3} = 152.6$ Hz, $^2J_{P4,5\text{-}P1} = 26.7$ Hz, 2P).

Synthesis of $[P_5Br_2]^+[Al(OR)_4]^-$ (4b): $Ag(CH_2Cl_2)[Al(OR)_4]^-$ (0.848 g, 0.731 mmol) was weighed into a two-bulbed glass vessel incorporating a fine-sintered glass frit and two J. Young valves. P_4 (0.086 g, 0.694 mmol) was added to the solid, then PBr_3 (0.188 g, 0.066 mL, 0.695 mmol) was added at 77 K, and CH_2Cl_2 (ca. 10 mL) was condensed onto the mixture and allowed to stir at −78 °C for 8 h. For completion of the reaction, the vessel was stored in a freezer at −80 °C for 10 days and occasionally heavily shaken. A clear colorless solution was obtained by filtration of the insoluble AgBr. The volume of the solvent was quickly reduced to about 1 mL at 0 °C. $[P_5Br_2]^+[A]^-$ crystallized in colorless blocks almost quantitatively from the cooled concentrated filtrate (−30 °C). Yield: 0.752 g (85 %). ^{13}C NMR (63 MHz, CD_2Cl_2, −70 °C): $\delta = 121.5$ (q, $J_{CF} = 292.0$ Hz, CF_3); ^{27}Al NMR (78 MHz, CD_2Cl_2, −70 °C): $\delta = 38.7$ (s, $\tilde{\nu}_{1/2} = 12$ Hz); ^{31}P NMR (101 MHz, CD_2Cl_2, −80 °C): $\delta = 162.0$ (dt, $^1J_{P2,3\text{-}P1} = 320.9$ Hz, $^1J_{P2,3\text{-}P4,5} = 148.7$ Hz, 2P), 20.0 (tt, $^1J_{P1\text{-}P2,3} = 320.9$ Hz, $^2J_{P1\text{-}P4,5} = 25.8$ Hz, 1P), −237.1 (td, $^1J_{P4,5\text{-}P2,3} = 148.7$ Hz, $^2J_{P4,5\text{-}P1} = 25.8$ Hz, 2P).

Reaction leading to $[P_2I_5(CS_2)]^+[(RO)_3Al\text{-}F\text{-}Al(OR)_3]^-$ (5): $Ag(CH_2Cl_2)[Al(OR)_4]$ (0.863 g, 0.744 mmol) and P_2I_4 (0.445 g, 0.782 mmol) were weighed into one bulb of a single-piece apparatus.[58] CS_2 (ca. 15 mL) was

condensed onto the solid mixture at 77 K, and the resulting suspension was stirred overnight at −30 °C. Apparently little had dissolved, and therefore CH_2Cl_2 (ca. 2 mL) was additionally condensed onto the suspension at 77 K. The resulting yellow solution over a little yellow precipitate (AgI) was stirred for 1 h at room temperature and filtered. The solution was concentrated to about 3 mL, and long yellow needles of $[P_2I_5(CS_2)]^+[(RO)_3Al\text{-}F\text{-}Al(OR)_3]^-$ (**1**) were isolated (0.587 g, 70 % based on Al). The Raman data of these crystals were incorporated into the text, NMR data of the crystals dissolved in CD_2Cl_2 (0.013 M solution): ^{13}C NMR (63 MHz, CD_2Cl_2, 25 °C): $\delta = 122.3$ (q, $J_{CF} = 284.4$ Hz, CF_3); ^{27}Al NMR (78 MHz, CD_2Cl_2, 25 °C): $\delta = 36.0$ (s, $\tilde{\nu}_{1/2} = 5$ Hz); ^{31}P NMR (101 MHz, CD_2Cl_2, 25 °C): not observed; ^{31}P NMR (101 MHz, CD_2Cl_2, −70 °C): $\delta =$ 91 (d, $^1J_{PP} = 382$ Hz, 2P), −2 (t, $^1J_{PP} = 382$ Hz, 1P) ($P_3I_6^+$; see text).

In situ NMR reaction according to Equation (6): $Ag(CH_2Cl_2)[Al(OR)_4]$ (0.186 g, 0.160 mmol) and P_2I_4 (0.092 g, 0.161 mmol) were weighed into a NMR tube glass-blown onto a valve. CD_2Cl_2 (0.7 mL) was condensed onto the mixture at 77 K, and the sealed tube was then stored at −30 °C and occasionally heavily shaken. Solid yellow AgI formed in a yellow solution. ^{31}P NMR spectra of this sample were recorded after 12 h and showed the signals of $P_2I_5^+$ (80 %, $\delta(^{31}P; -70\,^\circ C) = 126.1$ (d, $^1J_{PP} = 322$ Hz, 1P), −157.0 (d, $^1J_{PP} = 322$ Hz, 1P)) and $P_3I_6^+$ (20 %, $\delta(^{31}P; -70\,^\circ C) = 89.7$ (d, $^1J_{PP} =$ 381 Hz, 2P), −4.7 (t, $^1J_{PP} = 381$ Hz, 1P)).

In situ NMR reaction according to Equation (11): $[P_2Br_5]^+[Al(OR)_4]^-$ (0.104 g, 0.073 mmol) and P_4 (0.009 g, 0.073 mmol) were weighed into a NMR tube glass-blown onto a valve. CD_2Cl_2 (0.7 mL) was condensed onto the mixture at 77 K, and the sealed tube was then stored at −80 °C and occasionally heavily shaken. A slightly yellow solution resulted, but no precipitate was formed. ^{31}P NMR spectra of this sample were recorded after 5 days at −80 °C and showed the signals of $P_5Br_2^+$ (see above) and PBr_3 ($\delta(^{31}P) = 228$). The actual spectrum has been deposited.

X-ray crystal structure determinations: Data collection for X-ray structure determinations were performed on a STOE IPDS diffractometer by using graphite-monochromated $Mo_{K\alpha}$ (0.71073 Å) radiation. Single crystals were mounted in perfluoro ether oil on top of a glass fiber and then brought into the cold stream of a low-temperature device so that the oil solidified. All calculations were performed on PCs by using the SHELX97 software package. The structures were solved by direct methods and successive interpretation of the difference Fourier maps, followed by least-squares refinement. Compounds **3a**,**b** at 200 K were fourfold twinned and the anions of these structures were restrained by a set of about 100 SADI instructions. Within all of the many tested crystals of **3b** at 150 K some (tetragonal?) domains of another phase (cf. fourfold twinning of **3a**,**b** at 200 K) remained, and reflections of this phase were visible in all of the collected images. Therefore, the intensities of 1600 of the 7000 unique reflections were affected by reflections of the other phase and had to be omitted manually by using the OMIT command in SHELXL97. With the 5406 remaining less- or unaffected unique reflections, the structure was refined to a final $R1$ (w$R2$) value of 0.0876 (0.1634). The monoclinic crystals of **4b** with a β angle of 90.15(3)° might possibly be twinned, with a mirror plane being the twin element. However, despite many attempts, we were unable to find the twinning law. Upon cooling the crystals of **4b** from 200 to 150 K, a phase transition occurred, and all of the many tested crystals of **4b** were destroyed. One crystal lasted for about 7 images, and a unit-cell determination of this crystal showed it to be truly monoclinic with a β angle of 94.5° and similar lattice constants to the 200 K structure. However, this crystal was also destroyed by the strain imposed on it after the phase transition. Therefore the data for **4b** could not be collected at lower temperatures, so that the thermal parameters of the anion and the agreement factors of the structure remained relatively high. Although cooled to 170 or 150 K, many of the CF_3 groups in **5′** and **5″** were still rotating, and therefore a series of SADI restraints was used to keep the CF_3 groups in place. Several fluorine and carbon atoms had to be split over two positions and were included isotropically in the refinement with occupation factors of 20 to 40 % for the disordered positions. All other atoms were refined anisotropically. Relevant data concerning crystallographic data, data collection, and refinement details are compiled in Table 15. CCDC-179450–179456 (**1a**,**b**, **3a**,**b**, **5**) and CCDC-167142 (**4b**) contain the supplementary crystallographic data for this paper. These data can be obtained free of charge via www.ccdc.cam.ac.uk/conts/retrieving.html (or from the Cambridge Crystallographic Data Centre, 12 Union Road, Cambridge CB2 1EZ, UK; fax: (+44) 1223-336-033; or deposit@ccdc.cam.uk).

Computational details: All computations were done with the program TURBOMOLE.[59] The geometries of all species were optimized at the (RI-)MP2 level[60] with triple ζ valence polarization (two d and one f functions)

Table 15. Crystallographic and refinement details.

Compound	**1a**	**1b**	**3a** (200 K)	**3b** (200 K)	**3b** (150 K)	**4b**	**5′**	**5″**
Cryst size [mm]	0.6 × 0.3 × 0.3	0.6 × 0.1 × 0.1	0.4 × 0.3 × 0.3	0.4 × 0.4 × 0.4	0.5 × 0.4 × 0.4	0.3 × 0.3 × 0.5	0.1 × 0.2 × 0.5	0.5 × 0.3 × 0.3
Crystal system	tetragonal	tetragonal	triclinic	triclinic	triclinic	monoclinic	triclinic	triclinic
Space group	$I\bar{4}$	$I\bar{4}$	$P\bar{1}$	$P\bar{1}$	$P\bar{1}$	$P2/n$	$P\bar{1}$	$P\bar{1}$
a [Å]	13.978(2)	13.6400(19)	9.778(3)	9.6937(19)	9.829(2)	13.536(3)	10.493(2)	10.462(2)
b [Å]	13.978(2)	13.6400(19)	14.501(3)	14.016(3)	13.702(3)	9.554(2)	12.715(3)	12.696(3)
c [Å]	9.405(2)	9.4489(19)	14.519(3)	14.016(3)	13.906(3)	14.508(3)	23.237(5)	23.358(5)
α [°]	90	90	90.00(3)	90.00(3)	90.79(3)	90	80.56(3)	80.31(3)
β [°]	90	90	90.00(3)	90.00(3)	94.08(3)	90.15(3)	79.13(3)	77.63(3)
γ [°]	90	90	90.00(3)	90.00(3)	90.31(3)	90	76.16(3)	76.20(3)
V [Å^3]	1837.4(5)	1758.0(5)	2058.6(7)	1904.3(7)	1867.9(6)	1876.2(6)	2933.2(10)	2920.6(10)
Z	2	2	2	2	2	2	2	2
ρ(calcd) [Mg m^{-3}]	2.722	2.489	2.684	2.492	2.540	2.269	2.554	2.565
μ [mm^{-1}]	3.671	4.870	4.067	5.589	5.689	2.61	3.021	3.021
Max./min. Trans.	0.421/0.215	0.582/0.791	0.625/0.731	0.438/0.701	0.365/0.670	0.230/0.429	0.504/0.809	0.879/0.653
Index range	$-17 \le h \le 17$	$-16 \le h \le 9$	$-11 \le h \le 11$	$-9 \le h \le 11$	$-12 \le h \le 12$	$-16 \le h \le 16$	$-11 \le h \le 11$	$-12 \le h \le 12$
	$-16 \le k \le 16$	$-16 \le k \le 13$	$-17 \le k \le 17$	$-17 \le k \le 17$	$-15 \le k \le 16$	$-11 \le k \le 11$	$-15 \le k \le 15$	$-15 \le k \le 15$
	$-11 \le l \le 11$	$-11 \le l \le 11$	$-17 \le l \le 17$	$-17 \le l \le 17$	$-17 \le l \le 17$	$-17 \le l \le 16$	$-28 \le l \le 28$	$-28 \le l \le 28$
2θ [°]	51.44	51.80	51.84	51.76	51.78	51.96	51.98	51.92
T [K]	150	200	200	200	150	200	170	150
Refl. Collected	6490	3445	16061	9802	11479	14525	23335	21764
Refl. Unique	1710	1457	7375	6517	5406	3469	10691	10395
Refl. Observed (2σ)	1705	1282	4964	3305	2951	2323	5891	8036
R (int.)	0.0464	0.0973	0.0570	0.0556	0.1635	0.0577	0.0554	0.0475
GOOF	1.124	1.035	0.988	0.938	0.918	1.082	0.880	1.074
Final R (2σ)	0.0222	0.0633	0.0670	0.0713	0.0876	0.0957	0.0763	0.0736
Final $wR2$	0.0556	0.1674	0.1722	0.1678	0.1634	0.2823	0.1911	0.2226
$\Delta\rho$ (max/min) [e Å^{-3}] (near I)	0.653	0.876	1.244	1.038	0.988	0.853	1.646	1.254 (near anion)

0947-6539/02/0819-4490 $ 20.00+.50/0 *Chem. Eur. J.* **2002**, *8*, No. 19

TZVPP basis set.[61] The 28 and 46 core electrons of Ag and I were replaced by a quasi-relativistic effective core potential.[62] All species were also fully optimized at the BP86/SV(P) (DFT) level, although these geometries are not shown and are only discussed in a few cases. Approximate solvation energies (solution in CH_2Cl_2 with $\varepsilon_r = 8.92$) were calculated with the COSMO model[63] at the BP86/SV(P) (DFT) level by using the MP2/TZVPP geometries. Frequency calculations were performed for all species, and, if not stated otherwise, all structures represent true minima without imaginary frequencies on the respective hypersurface. For thermodynamic calculations the zero point energy and thermal contributions to the enthalpy and the free energy at 298 K or other given temperatures have been included.[44] The calculation of the thermal contributions to the enthalpy and entropic contributions to the free energy were done with Gaussian98W.[64] For all species, a modified Roby–Davidson population analysis was performed by using the MP2/TZVPP electron density.

Acknowledgements

We thank Prof. H. Schnöckel and for valuable discussions and advice, Dr. H. Himmel; Dipl. Chem. G. Stösser and Dipl. Chem. J. Bahlo for recording the Raman and IR spectra, and Dr. E. Matern and H. Berberich for their patience in recording the many low-temperature NMR spectra. Financial support from the German Science Foundation DFG as well as a Liebig grant and financial support from the Fond der Chemischen Industrie are gratefully acknowledged.

[1] a) J. Passmore, *J. Chem. Soc. Dalton Trans.* **1978**, 1251; b) C. Aubauer, M. Kaupp, T. M. Klapötke, H. Nöth, H. Pietrowski, W. Schnick, J. Senker, *J. Chem. Soc. Dalton Trans.* **2001**, 1880, and references therein.
[2] S. Pohl, *Z. Anorg. Allg. Chem.* **1983**, *498*, 20.
[3] a) C. Aubauer, G. Engelhardt, T. M. Klapötke, A. Schulz, *J. Chem. Soc. Dalton Trans.* **1999**, 1729; b) C. Aubauer, T. M. Klapötke, P. M. Mayer, *Acta Crystallogr.* **2001**, *E57*, i1.
[4] I. Krossing, *J. Chem. Soc. Dalton Trans.* **2002**, 500.
[5] B. W. Tattershall, N. L. Kendall, *Polyhedron* **1994**, *13*, 1517.
[6] I. Thornieport-Oetting, T. Klapötke, *Chem. Commun.* **1990**, 132.
[7] See for example: a) D. D. Wagman, W. H. Evans, V. B. Parker, R. H. Schumm, I. Halow, S. M. Bailey, K. L. Churney, R. L. Nuttal, *J. Phys. Chem. Ref. Data*, **1982**, *11*, Suppl. 2; b) S. G. Lias, J. E. Bartmess, J. F. Liebman, J. L. Holmes, R. D. Levin, W. G. Mallard, *J. Phys. Chem. Ref. Data*, **1988**, *17*, Suppl. 1; c) *CRC Handbook of Chemistry and Physics* 76th ed., (Ed.: D. R. Lide), CRC Press, Boca Raton, **1996**; d) http://www.nist.gov/chemistry.
[8] S. M. Ivanova, B. G. Nolan, Y. Kobayashi, S. M. Miller, O. P. Anderson, S. H. Strauss, *Chem. Eur. J.* **2001**, *7*, 503.
[9] I. Krossing, *Chem. Eur. J.* **2001**, *7*, 490.
[10] I. Krossing, *J. Am. Chem. Soc.* **2001**, *123*, 4603.
[11] Only slightly more basic anions, that is, $Al[OC(CH_3)(CF_3)_2]_4^-$, lead to the formation of the molecular species $(P_4)AgAl[OC(CH_3)(CF_3)_2]_4$ in which the silver cation is coordinated by one P_4 molecule and two oxygen atoms from the anion.[12]
[12] I. Krossing, *Chem. Eur. J.* **2002**, *8*, 700.
[13] Here and elsewhere: containing one molecule of coordinated CH_2Cl_2.
[14] I. Krossing, I. Raabe, *Angew. Chem.* **2001**, *113*, 4544; *Angew. Chem. Int. Ed.* **2001**, *40*, 4406.
[15] Dissolved $PBr_4^+[Al(OR)_4]^-$ decomposes to intermediately give $ROPBr_4$ and $Al(OR)_3$. $ROPBr_4$ decomposes with formation of $OPBr_3$ and RBr; $OPBr_3$ and $Al(OR)_3$ react to the final product $Br_3PO \rightarrow Al(OR)_3$, which was characterized by X-ray analysis and NMR. However, this is subject to ongoing research and will be published elsewhere.
[16] S. Pohl, *Z. Anorg. Allg. Chem.* **1983**, *498*, 15.
[17] W. Gabes, K. Olie, *Acta Crystallogr. Sect. B* **1970**, *26*, 443.
[18] M. Gerken, P. Kolb, H. P. A. Mercier, H. Borrmann, D. A. Dixon, G. J. Schrobilgen, *Inorg. Chem.* **2000**, *39*, 2813.
[19] Upon cooling the crystal from 200 K to 150 K, a phase transition occurred, and all of the 10 tested crystals cracked, even when cooled very slowly. Therefore, the rotation of the 12 CF_3 groups could not be frozen out, and thermal ellipsoids of the anion are large and the agreement factors remained relatively high. Moreover the $P_5Br_2^+$ cation occupies two different positions, each with a 50% occupation (see Supporting Information).
[20] A search of the chemical abstracts data base with Scifinder and the Cambridge structural database CSD with the program Conquest did not reveal a precedent for this P_5 cage. However, similar C_{2v}-symmetric MP_4 units (i.e. M = Ir) formally containing a P_4^{2-} unit are known.[21]
[21] M. Scheer, U. Becker, E. Matern, *Chem. Ber.* **1996**, *129*, 721.
[22] H. Brands, R. Feuerhake, I. Krossing, S. Koenig, *J. Fluor. Chem.* **2001**, *112*, 83.
[23] H. K. Roobottom, H. D. B. Jenkins, J. Passmore, L. Glasser, *Inorg. Chem.* **1999**, *38*, 3609.
[24] T. S. Cameron, A. Decken, I. Dionne, M. Fang, I. Krossing, J. Passmore, *Chem. Eur. J.* **2002**, *8*, 3386–3401.
[25] I. Krossing, A. Adolf, M. Gonsior, *J. Am. Chem. Soc.* **2002**, *124*, 7111.
[26] $\Delta_f H(PI_2^+)$ followed from $\Delta_r H(PBr_2^+ + I_2 \rightarrow PI_2^+ + Br_2)$ of +26 kJ mol^{-1}, therefore $\Delta_f H(PI_2^+) = \Delta_f H(PBr_2^+) + \Delta_f H(I_2) - \Delta_f H(Br_2) + 26 = 862 + 62 - 31 + 26 = +919$ kJ mol^{-1}; $\Delta_f H(PI_3)$ followed from $\Delta_r H(PBr_3 + 1.5\,I_2 \rightarrow PI_3 + 1.5\,Br_2)$ of +97 kJ mol^{-1}, therefore $\Delta_f H(PI_3) = \Delta_f H(PBr_3) + 1.5\,\Delta_f H(I_2) - 1.5\,\Delta_f H(Br_2) + 97 = -91 + 93 - 47 + 97 = +52$ kJ mol^{-1}.
[27] a) $\Delta_r H(PBr_2^+ + Br_2 \rightarrow PBr_4^+)$ is −275 kJ mol^{-1}, therefore $\Delta_f H(PBr_4^+) = \Delta_f H(PBr_2^+) + \Delta_f H(Br_2) + (-275) = 862 + 31 - 275 = +617$ kJ mol^{-1}; b) $\Delta_r H(PBr_2^+ + PBr_3 \rightarrow P_2Br_5^+)$ is −192 kJ mol^{-1}, therefore $\Delta_f H(P_2Br_5^+) = \Delta_f H(PBr_2^+) + \Delta_f H(PBr_3) + (-192) = 862 + (-91) - 192 = +579$ kJ mol^{-1}; c) $\Delta_r H(PBr_2^+ + P_4 \rightarrow P_5Br_2^+)$ is −211 kJ mol^{-1}, therefore $\Delta_f H(P_5Br_2^+) = \Delta_f H(PBr_2^+) + \Delta_f H(P_4) + (-211) = 862 + 54 - 211 = +705$ kJ mol^{-1}.
[28] a) $\Delta_r H(PI_2^+ + I_2 \rightarrow PI_4^+)$ is −217 kJ mol^{-1}, therefore $\Delta_f H(PI_4^+) = \Delta_f H(PI_2^+) + \Delta_f H(I_2) + (-217) = 919 + 62 - 217 = +764$ kJ mol^{-1}; b) $\Delta_r H(PI_2^+ + PI_3 \rightarrow P_2I_5^+)$ is −222 kJ mol^{-1}, therefore $\Delta_f H(P_2I_5^+) = \Delta_f H(PI_2^+) + \Delta_f H(PI_3) + (-222) = 919 + 52 - 222 = +749$ kJ mol^{-1}; c) $\Delta_r H(PI_2^+ + P_4 \rightarrow P_5I_2^+)$ is −189 kJ mol^{-1}, therefore $\Delta_f H(P_5I_2^+) = \Delta_f H(PI_2^+) + \Delta_f H(P_4) + (-189) = 919 + 54 - 189 = +784$ kJ mol^{-1}.
[29] As observed earlier, large counterions lead to fluorescence and dilute the amount of Raman scatterer present (= number of P–X cations per volume). This additionally reduces the intensity of the presented spectra.
[30] a) C. Aubauer, T. M. Klapötke, A. Schulz, *Internet J. Vibr. Spec. [www.ijvs.com]* **1999**, *3*, 2, 4 (http://www.ijvs.com/volume3/edition2/section4.htm); b) C. Aubauer, T. M. Klapötke, *Internet J. Vibr. Spec. [www.ijvs.com]* **2001**, *5*, 4, 4 (http://www.ijvs.com/volume5/edition4/section2.htm).
[31] I–I contacts—as short as 3.435 Å[2] (the sum of the iodine van der-Waals radii is 4.40 Å)—presumably weaken the P–I bonds in the cation so that all the observed bands are shifted to lower energy relative to a "naked" $P_2I_5^+$ cation. This is shown for the position of the two most intense vibrations: in $P_2I_5AlI_4$ they are found at 210 and 127 cm^{-1}, in **3a** and **5** they are at 223 and 136/137 cm^{-1}.
[32] P: 6–31G(d,p), I: quasi-relativistic pseudopotential ECP46MWB, DZ + P valence electron description.
[33] However, the $Al(OR)_4^-$ anion has a strong IR band at 444 cm^{-1}; this makes the assignment of the vibration ambiguous.
[34] ω_3 and ω_4 in ref. [3] were calculated to appear at 350 and 354 cm^{-1} and were assigned to one band; therefore, the rest of the assignment is fortuitously correct. Consequently, ω_1 was assigned to a band at 390 cm^{-1} (exp.) that is actually ω_2, ω_2 was assigned to a band that is ω_3, and ω_3 and ω_4 were assigned jointly to a band that is actually only ω_4.
[35] J. R. Durig, J. M. Casper, *J. Mol. Struct.* **1970**, *55*, 351.
[36] M. Kaupp, C. Aubauer, G. Engelhardt, T. M. Klapötke, O. Malkina, *J. Chem. Phys.* **1999**, *110*, 3897.
[37] Neither lowering the temperature further to −105 °C nor raising the temperature to −20 °C (10 °C steps) and recording the NMR spectra between +1200 and −1000 ppm gave any sign of another, more highly oxidized phosphorus species. The m.p. of CD_2Cl_2 is −96 °C; however, supercooled solutions of **3a** could be measured for some time at this temperature (500 scans).
[38] With $K = ([P_3I_6]^+[PI_4]^+)/[P_2I_5]^+)^2 = 0.57$ and a given $P_2I_5^+$ concentration (c_A) of 1.0 mol L^{-1}, one expects a $P_3I_6^+$=PI_4^+ concentration (c_B) of 0.75 mol L^{-1} (or $0.75 \times c_A$). For $c_A = 0.1$ mol L^{-1}, c_B is 0.24 mol L^{-1} (or $2.4 \times c_A$), for $c_A = 0.01$ mol L^{-1}, c_B is 0.075 mol L^{-1} (or $7.5 \times c_A$), and for

$c_A = 0.001$ mol L^{-1}, c_B is 0.024 mol L^{-1} (or $24 \times c_A$). This shows that at low concentrations, as in the 0.013 M sample, the disproportionation side is favored, and that at higher concentrations, such as in the 0.095 M sample, both sides of Equation (7) are visible.

[39] a) Review: J. Passmore, *The Chemistry of Inorganic Ring Systems*, *Vol. 14* (Ed.: R. Steudel), **1992**, Elsevier Science Publisher, p. 373; b) W. A. S. Nandana, J. Passmore, P. S. White, C.-M. Wong, *Inorg. Chem.* **1989**, *28*, 3320.

[40] a) S. Brownridge, H. D. B. Jenkins, I. Krossing, J. Passmore and H. K. Roobottom, *Coord. Chem. Rev.* **2000**, *197*, 397; b) T. S. Cameron, R. J. Deeth, I. Dionne, H. D. B. Jenkins, I. Krossing, J. Passmore, H. Roobottom, *Inorg. Chem.* **2000**, *39*, 5614; c) I. Krossing, J. Passmore, unpublished results.

[41] H. Althaus, H. J. Breunig, E. Lork, *Chem. Commun.* **1999**, 1971.

[42] M. Hesse, H. Maier, B. Zeeh, *Spektroskopische Methoden in der organischen Chemie*, 4th ed. **1991**, Thieme, Stuttgart, p. 96.

[43] Solvation energies were obtained from the MP2/TZVPP geometries by using the COSMO model at the BP86/SVP level and a dielectric constant for CH_2Cl_2 of 8.92.

[44] Thermal and entropic contributions to the enthalpy and free energy were obtained by fully optimizing all the species in question with Gaussian98W at the semiempirical PM3 level. Contributions at nonstandard temperatures, i.e. 193 and 243 K, were obtained by using the FREQ = ReadIsotopes option in Gaussian98W. All these species also represented true minima without imaginary frequencies at the PM3 level. ZPEs were taken from the MP2 calculation. Since statistical thermodynamics are only little influenced by the employed geometries, and the entropic contributions mainly arise from the moment of inertia of a species, it is believed that errors associated with this procedure are very small if it is used consistently.

[45] For PBr_2^+ and PBr_3, only $\Delta_f H(PBr_2^+)$ at 0 K was available.[53] The thermal contributions to the enthalpy at 298 K of 19 kJ mol^{-1} (PBr_2^+) and 24 kJ mol^{-1} (PBr_3) were therefore calculated by Gaussian98[44] and added to the 0 K values of 843 and -115 kJ mol^{-1} to give $\Delta_f H(PBr_2^+, 298\ K) = 862$ kJ mol^{-1} and $\Delta_f H(PBr_3, 298\ K) = -91$ kJ mol^{-1}. The 298 K enthalpies of formation of P_3^+, Br_2, and P_4 are 1006, 31, and 54 kJ mol^{-1},[7] giving the reaction enthalpy of Equation (11) as $\Delta_r H[\text{Eq. (11)}] = 862 + 27 - 1006 - 31 = -148$ kJ mol^{-1}.

[46] W. W. Du Mont, F. Ruthe, *Coord. Chem. Rev.* **1999**, *189*, 101.

[47] N. Burford. T. S. Cameron, J. A. C. Clyburne, K. Eichele, K. H. Robertson, S. Sereda, R. E. Wasylishen, W. W. Whitla, *Inorg. Chem.* **1996**, *35*, 5460.

[48] This is also reflected in the MP2-calculation: *d*(P–P) = 2.253 (I) and 2.264 (Br); *SEN*(P–P) = 1.05 (I) and 1.01 (Br).

[49] Performed with the program Gaussian98.[64] Vibrational frequencies were assigned based on the visualization of the modes with the program GaussView.

[50] C. Adamo, V. Barone, *J. Chem. Phys.* **1998**, *108*, 664.

[51] D. Gudat, *Eur. J. Inorg. Chem.* **1998**, 1087.

[52] Calculated with our assessed thermochemical volume of $P_2I_5^+$ of 271 Å^3 and the known thermochemical volume of AsF_6^- of 110 Å^3, and by using Jenkins' volume-based formula.[23]

[53] O. A. Mazyar, T. Baer, *Chem. Phys. Lett.* **1998**, *288*, 327.

[54] a) L. Latifzadeh-Masoudipour, K. Balasubramanian, *Chem. Phys. Lett.* **1997**, *267*, 545; b) L. Latifzadeh, K. Balasubramanian, *Chem. Phys. Lett.* **1996**, *258*, 393; c) L. Latifzadeh, K. Balasubramanian, *Chem. Phys. Lett.* **1995**, *241*, 13.

[55] I.-C. Hwang, K. Seppelt, *Angew. Chem.* **2001**, *113*, 3803; *Angew. Chem. Int. Ed.* **2001**, *40*, 3690.

[56] a) J. Beck, *Angew. Chem.* **1994**, *106*, 172; *Angew. Chem. Int. Ed. Engl.* **1994**, *33*, 163; b) J. Beck, *Coord. Chem. Rev.* **1997**, *163*, 55.

[57] No precipitate was visible even after storage for weeks at $-80\,^\circ$C in solutions of **3a** in CH_2Cl_2 (ca. 0.1 M).

[58] This apparatus incorporates two bulbs (closed with J. Young valves) connected by a glass tube including a fine glass frit (U-shaped). The product side also included an additional valve that allowed the direct preparation of NMR samples of the reaction solution.

[59] TURBOMOLE, Version 5: a) R. Ahlrichs, M. Bär, M. Häser, H. Horn, C. Kölmel, *Chem. Phys. Lett.* **1989**, *162*, 165; b) M. v. Arnim, R. Ahlrichs, *J. Chem. Phys.* **1999**, *111*, 9183.

[60] F. Weigend, M. Häser, *Theor. Chim. Acta* **1997**, *97*, 331.

[61] a) A. Schäfer, H. Horn, R. Ahlrichs, *J. Chem. Phys.* **1992**, *97*, 2571; b) A. Schäfer, C. Huber, R. Ahlrichs, *J. Chem. Phys.* **1994**, *100*, 5829.

[62] W. Kuechle, M. Dolg, H. Stoll, H. Preuss, *Mol. Phys.* **1991**, *74*, 1245.

[63] A. Klamt, G. Schürmann, *J. Chem. Soc. Perkin. Trans.* **1993**, *2*, 799.

[64] *Gaussian 98* (Revision A.3), M. J. Frisch, G. W. Trucks, H. B. Schlegel, G. E. Scuseria, M. A. Robb, J. R. Cheeseman, V. G. Zakrzewski, J. A. Montgomery, R. E. Stratmann, J. C. Burant, S. Dapprich, J. M. Millam, A. D. Daniels, K. N. Kudin, M. C. Strain, O. Farkas, J. Tomasi, V. Barone, M. Cossi, R. Cammi, B. Mennucci, C. Pomelli, C. Adamo, S. Clifford, J. Ochterski, G. A. Petersson, P. Y. Ayala, Q. Cui, K. Morokuma, D. K. Malick, A. D. Rabuck, K. Raghavachari, J. B. Foresman, J. Cioslowski, J. V. Ortiz, B. B. Stefanov, G. Liu, A. Liashenko, P. Piskorz, I. Komaromi, R. Gomperts, R. L. Martin, D. J. Fox, T. Keith, M. A. Al-Laham, C. Y. Peng, A. Nanayakkara, C. Gonzalez, M. Challacombe, P. M. W. Gill, B. G. Johnson, W. Chen, M. W. Wong, J. L. Andres, M. Head-Gordon, E. S. Replogle, J. A. Pople, Gaussian, Inc., Pittsburgh PA, **1998**.

Received: February 22, 2002 [F3894]

  0947-6539/02/0819-4492 $ 20.00+.50/0